A METHOD TO ESTIMATE THE COOLING TIME OF ULTRA-RELATIVISTIC ELECTRONS IN PULSAR WIND NEBULAE

KATHALUWA LIYANAGE ISURU GUNAWARDHANA

A dissertation submitted in partial fulfilment of the requirements for the Bachelor of Science Special Degree in Physics

of the

University of Colombo, Sri Lanka

FEBRUARY 2015

DECLARATION

I certify that this dissertation does not incorporate without acknowledgement, any material previously submitted for a Degree or Diploma in any university and to the best of my knowledge and belief it does not contain any material previously published or written or oral communicated by other person except where due reference is made in the text.

.....

(Signature of candidate)

Isuru Gunawardhana

Index Number: S 10606

Reg. Number: 2010/s/12143

Date of submission:

ACKNOWLEDGEMENTS

It is with great pleasure I am using this opportunity to convey my sincere gratitude to everyone who supported me throughout the preparation and completion of this research.

I am really thankful and indebted to my supervisors: Prof. K. P. S. C. Jayaratne at Department of physics, University of Colombo, Sri Lanka and Dr. A.U. Abeysekara, at Departments of Physics & Astronomy, University of Utah, USA and Research Scientist Mr. Janaka Adassuriya at Astronomy and Space Science Division, Arthur C Clarke Institute for Modern Technologies, Katubedda, Sri Lanka, for their aspiring guidance, invaluable constructive criticism, unlimited knowledge extended and very insightful suggestions and supervision for the success of this research. Also I am sincerely grateful to them for sharing their truthful and illuminating views on a number of issues related to this research.

Last but not least, I thank all other persons unnamed, who gave invaluable support tofinish this researchproject successfully, including my parents who offered me invaluable moral support throughout my life.

ABSTRACT

Pulsar is a highly magnetized rotating neutron star. It continuously emits a wind of relativistic electrons and positrons. This wind creates an electron-positron-cloud around the pulsar. This cloud, which is full of relativistic electrons and positrons, is called a Pulsar Wind Nebula (PWN). As of 2014, 33 Pulsar Wind Nebulae (PWNe) have been detected in the TeV energy band. Current understanding is, these TeV photons are produced from up-scattering low-energy photons to high-energies by ultra-relativistic electrons and positrons in PWNe, which is a non-thermal process. This process is known as inverse-Compton scattering. During inverse-Compton scattering, ultra-relativistic electrons lose their energy and cool-down to low-energies. The average time that an ultra-relativistic electron takes to cool-down by inverse-Compton scattering is called the cooling time. Estimation of cooling time is important to understand how the luminosity of a PWN changes with time.

This thesis describes a statistical method developed for estimating the cooling time of ultra-relativistic electrons in a given PWN. This new method is a model independent technique. Cooling time was estimated as a function of two parameters: k and γ. Here k is the high-energy electron fraction in PWN and γ is the Bulk Lorentz Factor of electrons in the PWN. The estimated cooling time is proportional to k and inversely proportional to γ.

The developed method was applied to four PWNe: MSH 15-52, HESS J1420-607, HESS J1825-137 and HESS J1837-069. The estimated cooling times vary between 1.56 kyr (1000 years) to 1000 kyr for MSH 15-52, 13 kyr to 8000 kyr for HESS J1420-607, 21.4 kyr to 10000 kyr for HESS J1825-137 and 22.7 kyr to 15000 kyr for HESS J1837-069. Other researchers have found that the cooling time should be in thousand year (kyr) scale by using various approximations. The above obtained results verify that the new method developed here can be used to estimate the cooling time of ultra-relativistic electrons in Pulsar Wind Nebula.

TABLE OF CONTENTS

TABLE OF FIGURES

LIST OF TABLES

ABBREVIATIONS

HESS.....High Energy Stereoscopic System

IACTs.....Imaging Atmospheric Cherenkov Telescopes

IR.....Infra-Red

LAT.....Large Area Telescope

MHD.....Magneto Hydro Dynamic

ODE .....Ordinary Differential Equation

PWN..... Pulsar Wind Nebula

PWNe..... Pulsar Wind Nebulae

SED.....Spectral Energy Distribution

SN.....Supernova

SNRs.....Supernova Remnants

1. INTRODUCTION

1.1 Background of the study

Astronomy is believed as the oldest of all the sciences. It differs from all other sciences because it is not possible to carry out experimental tests in a laboratory. An astronomer can only observe what he/she sees in the outer space, and see whether observations are consistent with theories. Many cultures throughout the world starting from ancient Babylon (in 2^{nd} and 3^{rd} millennia BC) practiced astronomy. All of them made careful observations of the sky and recorded the patterns of stars using stones.

At present, scientists have found how stars get created, evolve and where they go after death. It is a circular process. Stars born inside molecular clouds, which are composed with relatively dense concentration of gas and dust. These regions are extremely cold. This extremely low temperature causes gas to clump into high densities. When the density reaches a certain point, star gets formed. The dense regions are called as "dark nebula". Dark nebula is opaque to visible eye. However infrared (IR) and radio telescopes can be used to investigate dark nebula. The formation of stars proceeds when the denser part of the cloud core collapses under its own gravity. As the cloud collapses, the material at the centre begins to heat up. This hot core at the centre of the collapsing cloud is known as a protostar.

Stars are fuelled by the nuclear fusion of hydrogen to form helium, deep in their interiors. The outflow of energy from the central regions of a star provides the pressure to keep the star in an equilibrium state. In other words, gravitational force is balanced by the pressure. Stars can be classified using their color and magnitude. These two quantities are plotted against each other. This forms color-magnitude (C-M) or Hertzsprung-Russell (H-R) diagram. The typical H-R diagram is shown in Figure 1. The main feature of this diagram is that most of the stars which are plotted lie on a diagonal line from top left to bottom right. This is called the Main sequence. As shown in Figure 1, Main Sequence stars span a wide range of luminosities and colors, and can be classified according to those characteristics. Our sun lies approximately in the middle of the main sequence and it requires about 50 million years, to mature from the beginning of the collapse to adulthood. Our Sun will stay in this mature phase (on the main sequence as shown in Figure 1) for approximately 10 billion years. The smallest stars, known as red dwarfs, may contain as little as 10% the mass of the Sun and at temperatures between 3000-4000 K. The most massive stars, known as hypergiants, may be 100 or more times more massive than the Sun, and have surface temperatures of more than 30,000 K.

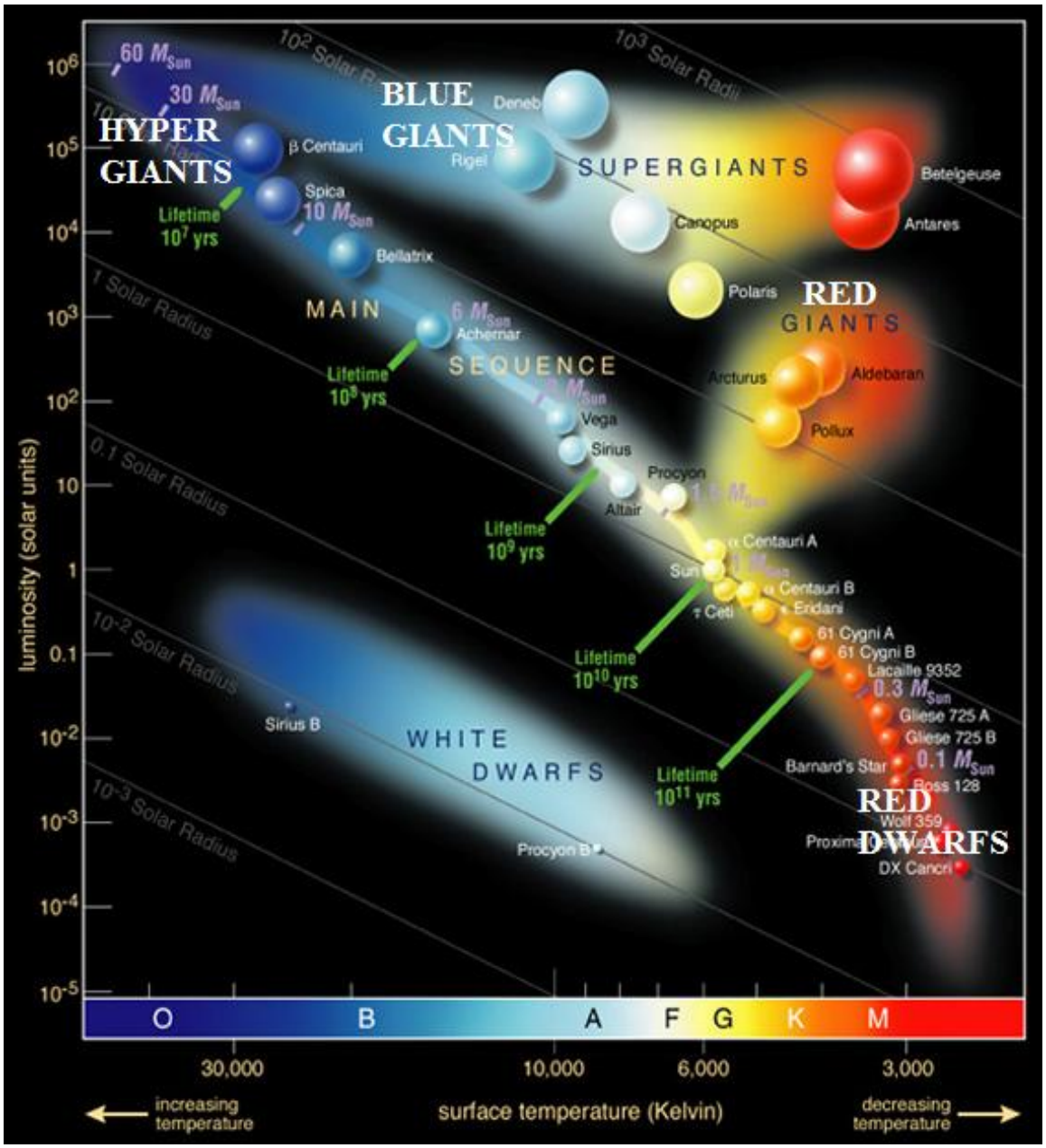

Figure 1.1: Hertzsprung-Russell diagram (Hertzsprung-Russell diagram plots stars by luminosity (vertical axis) and temperature or spectral class (horizontal axis). The grey color diagonal lines are lines of constant radius. The hotter (blue color) stars lie to the left and the cooler (red color) stars lie to the right of the above graph. The sun is used to define astronomical units; mass of the sun is 1 solar mass, radius of the sun is 1 solar radius and luminosity of the sun is 1 solar luminosity. Sun is a yellow G-type star, now on the main sequence.) (Adapted from: http://astronomer.wpengine.netdna-cdn.com/wp-content/uploads/2009/01/hrdiagram.jpg)

When stars have finished burning their nuclear fuel; they collapse due to their own gravity and then explode, which are called supernova explosions. Supernova explosions could produce neutron stars, or a black hole. The fact that which one of these 2 categories is produced after a supernova explosion depends on the mass of the star when it is in the main sequence. If a star has 1.5 to 5 times mass of the Sun, it will compact into **neutron stars** and a star with mass greater than 5 times the Sun's gets crush into a single point called **a black hole**. The following Figure 1.2 is illustrated these 2 situations clearly.

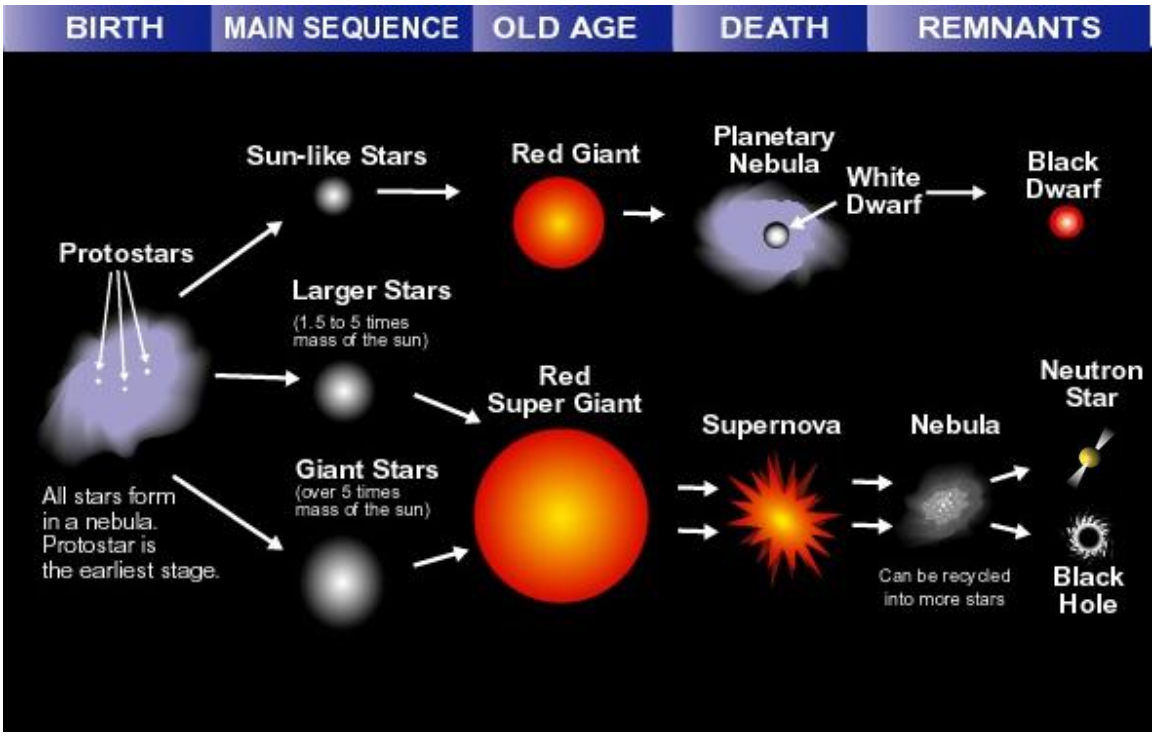

Figure 1.2: Life cycle of stars (Source**:** http://leescience8.wikispaces.com/Unit+Four)

A neutron star is about 20 km in diameter and has the mass of about 1.4 times that of our sun. Some neutron stars appear to be as pulsating objects called pulsars. Pulsars produce two photon jets along the magnetic dipole axis. This photon jet is visible to earth only when the jet is pointed towards the earth and not visible when it is pointing away from the earth. These two incidents are illustrated in the Figure 1.3.

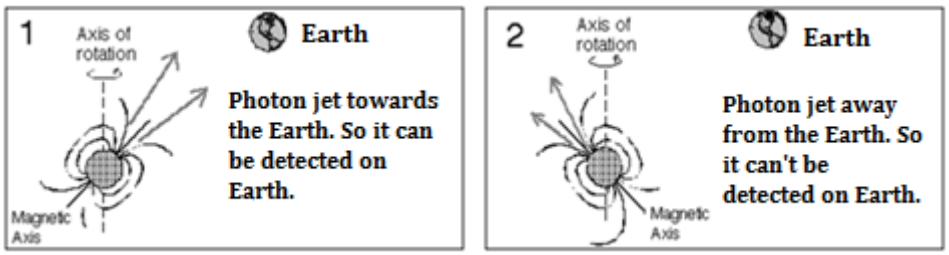

Figure 1.3: Basic two form of the photon jet related to Earth (Adapted from: Zeilik and Gaustad 1990)

Also Pulsars produce an out-flowing wind of relativistic electrons and positrons, known as pulsar wind. Pulsar wind create, cloud of electron/positron around the pulsar, which is known as Pulsar Wind Nebula (PWN). The term, nebulae is the plural term of nebula. The outgoing Pulsar wind is illustrated in the Figure 1.4 using blue color spiral shape rings. Pulsar keeps releasing high energy electron/positron into PWN using the Pulsar wind. Therefore PWN get powered by the pulsar wind of the associated pulsar.

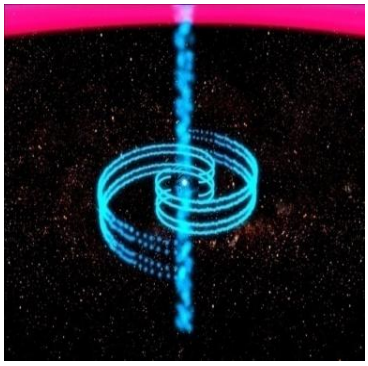

Figure 1.4: The Pulsar wind (Source: http://chandra.harvard.edu/photo/2002/0052/PulsarWind-105.jpg)

PWN is usually associated with the non-thermal emission from a magnetized plasma of relativistic electrons/positrons fed by pulsar wind (see Figure 1.5). If the Pulsar is young, the wind is surrounded by debris of Supernova explosion, which expand at a much lower (non-relativistic) velocity. When the wind impacts on the Supernova Remnants (SNRs) initially, a reverse shock is launched towards the Pulsar, which slows down the wind and transforms its bulk energy into a magnetized and ultra- relativistic Plasma. In this magnetized plasma of relativistic particles, low energy photons can be up scattered by the electrons/positrons to very high energies via the inverse-Compton Scattering effect.

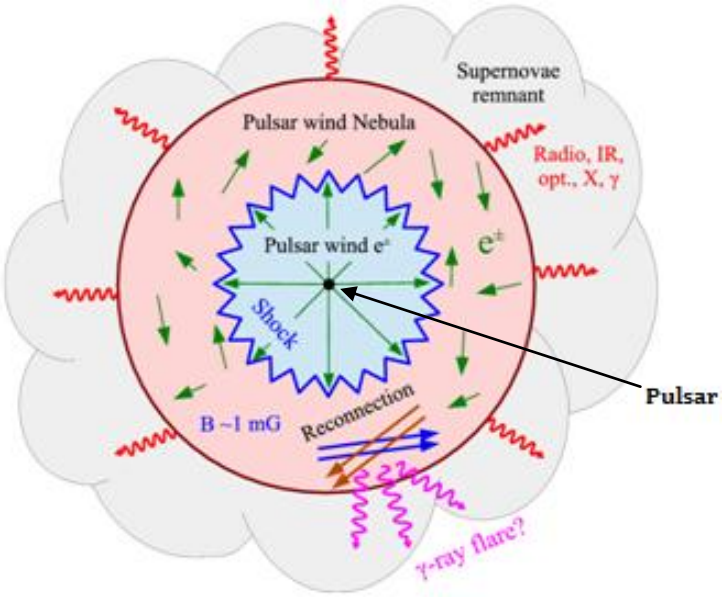

Figure 1.5: 2D diagram of the PWN and associated Pulsar (Adapted from: inspirehep.net)

Inverse-Compton Scattering is the inverse of the famous phenomena of Compton Scattering. The process is called inverse because the electrons lose energy rather than the photons. Inverse Compton scattering associates the scattering of low energy photons to high energies by ultra-relativistic electrons, so that the photons gain and the electrons lose energy.

At present, 33 TeV PWNe were detected (TeVCat, 2014). Current understanding is these TeV Photon are produced by the inverse-Compton Scattering. During the inverse-Compton Scattering process, low-energy photons become high-energy photons by the ultra-relativistic electrons and positrons in PWNe. Also in the same time ultra-relativistic electrons lose their energy and cool-down to low-energies. The average time that an ultra-relativistic electron takes to cool-down by inverse-Compton scattering is called as the cooling time.

1.2 Objective of the study

The objective of this study is developing a new statistical method to estimate the inverse-Compton Scattering cooling time of ultra-relativistic electrons in Pulsar Wind Nebulae, and estimating the cooling time of four TeV PWNe using the technique developed. Estimation of cooling time is important to understand how the luminosity of a PWN changes with the time.

1.3 Organization of the study

This thesis composed with 6 chapters. **Chapter 1** gives a brief introduction related to the background of the research and **Chapter 2** includes the Literature Review elucidates the previous studies related to this study and present study of this research. **Chapter 3** depicts the theoretical background regarding Neutron star, Pulsar, Pulsar Wind Nebula (PWN), cooling time, novel method of estimating cooling time and the methodology of obtaining k-γ phase space of cooling time. Then **Chapter 4** demonstrate the Data Analysis and Results which construes the sub topics of Pulsar properties, Fitted SED curves of four PWNe, cooling time values of the four PWNe, error calculation of cooling time and k-γ phase space graphs of cooling time of the four selected PWNe. **Chapter 5** describes the limitations of this study, difficulties which arise during the time of conducting the research and the accuracy of the developed method. Finally, **Chapter 6** concludes the final outcomes of the study.

2. LITERATURE REVIEW

2.1 Previous studies relating to this Research

In 1934, the existence of neutrons stars was proposed by astrophysicists Walter Baade & Fritz Zwicky (Baade & Zwicky, 1934). Sun like stars will not form neutron stars. Only massive stars (at least 1.5 times larger than our sun) will undergo a supernova explosion and become neutron stars. In 1939, the first equation of state of neutron star was evaluated by J.R. Opppenheimer & G. Volkoff (Oppenheimer & Volkoff, 1939). Then in 1967, F. Pacini (Pacini, 1967) proposed that the electromagnetic waves come from highly magnetized rotating neutron stars. Also he proposed that the Crab nebula was powered by such a star. The first pulsar was discovered by Jocelyn Bell and Anthony Hewish in 1967 who were studying interplanetary scintillation at Cambridge at that time. The pulsar discovered by Bell and Hewish is now called PSR B1919+21: PSR stands for Pulsating source of Radio and B1919+21 indicates the position of the pulsar in the sky. The observed recording in 1967 is shown in Figure 2.1.

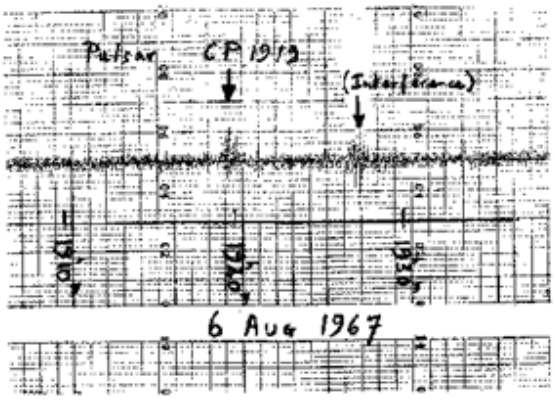

Figure 2.1: Discovery observations of the first pulsar. (The first recording of PSR 1919+21; the signal resembled the radio interference also seen on this chart) (Source: Lyne & Graham 1990)

In 1968, Pacini's proposed theories were confirmed by Bell and Hewish (Hewish & Bell, 1968) using the first discovered pulsar in 1967. The following Figure 2.2 shows the Jocelyn Bell and the radio telescope which was used to discover pulsars in 1967.

Figure 2.2: Jocelyn Bell in front of the radio telescope in 1967 (Source: http://nmsi.ac.uk)

About 1800 pulsars were detected using radio detectors in the end of 2010 (Imagine, 2014). However, only about 70 pulsars were detected using gamma-ray telescopes (Imagine, 2014). More than two-thirds of the currently known pulsars were discovered using the Parkes radio telescope in Australia (Hobbs, 2014). The following Figure 2.3 shows the Parkes radio telescope in Australia. Also the gigantic radio telescope in Puerto Rico, the Green Bank telescopes in America, the Molonglo telescope in Australia and the Jodrell Bank telescope in England were used to detect pulsars.

Figure 2.3: The Parkes radio telescope in Australia (Source: *John Sarkissian* (*CSIRO*))

The most well-known and also a prototypical PWN is "**The Crab nebula"** (Hester et al., 2008). The Crab nebula was associated with a supernova (SN) explosion observed in 1054 CE (Stephenson & Green, 2002). In the beginning, a 16th magnitude star embedded in the Crab Nebula was long presumed to be the stellar remnant and central engine (Minkowski, 1942; Pacini, 1967). This was confirmed by after the 33 ms optical and radio pulsations were detected from this star in the late 1960s (Cocke, Disney & Taylor, 1969; Staelin & Reifenstein, 1968) and then these pulsations were shown to be slowing down at a rate of 36 ns per day (Richards & Comella, 1969). So scientist concluded that the Crab nebula contains a rapidly rotating young neutron star (pulsar) formed in the SN of 1054 CE. This is the way by which the connection between pulsar and pulsar wind nebula was discovered. The following figure 2.4 shows the multi wavelength image of the Crab nebula.

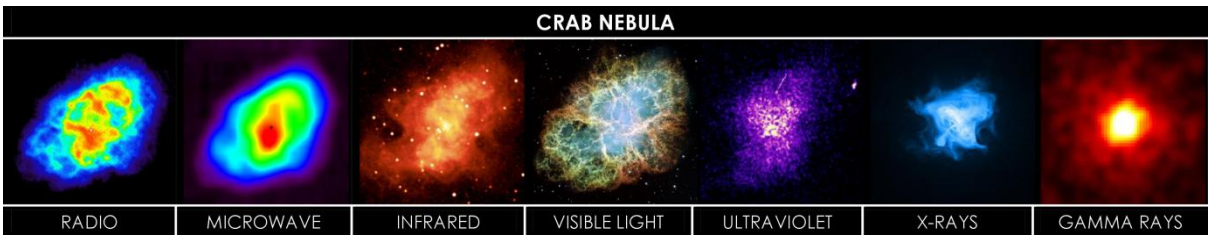

Figure 2.4: Multi wavelength image of the Crab nebula (Source: http://commons.wikimedia.org/wiki/File:Crab_Nebula_in_multiwavelength.png)

According to the above discovery, a theoretical understanding was soon developed in which the central pulsar generates a magnetized particle wind. This wind was composed of electron and positrons. These charge particles were accelerated to relativistic speed by the rapidly rotating super strong magnetic field of the spinning pulsar. Magneto Hydro Dynamic (MHD) models were used to explain the structure of the PWNe. MHD is the study of the dynamics of electrically conducting fluids (e.g. plasmas, electrolytes etc). The field of MHD was found by Hannes Alfven (Alfvén, 1942). The basic concept behind the MHD is that magnetic fields can induce currents in a moving conductive fluid. The present 2D MHD models were used to explain the high energy morphology of the PWNe. However they are not free of problems. So the first 3D studies are now established to overcome the problems which were arisen in the 2D MHD model.

The new generation of ground-based Imaging Atmospheric Cherenkov Telescopes (IACTs, e.g: High Energy Stereoscopic System, "HESS") have now begun to detect PWNe in the TeV band. The current structure of the PWNe was defined with as magnetized plasma and which is thought to consist mainly of energetic electrons/positrons (Gaensler & Slane, 2006). These electrons/positrons emit non-thermal radiation over a wide energy range. Current understanding is, TeV photons are produced from up-scattering of low-energy photons to high-energies by the ultra-relativistic electrons and positrons in PWNe, which is a non-thermal process. This process is known as inverse-Compton scattering.

2.2 Present study

This study reports a statistical method developed for estimating the inverse-Compton scattering cooling time of ultra-relativistic electrons in PWNe. The cooling time of four PWNe was estimated using this statistical method. This newly developed method is a model independent technique. So, it can be used to estimate the cooling time of any PWN easily. The following Table 2.1 shows the four PWNe and their associated pulsars which were used in this study.

Table 2.1: Selected four TeV PWNe and their associated Pulsars

Name of the TeV PWNe	Name of the associated Pulsar
MSH 15-52 (Aharonian et al., 2005)	PSR B1509-58
HESS J1420-607 (Aharonian et al., 2006b)	PSR J1420-6048
HESS J1825-137 (Aharonian et al., 2006c)	PSR J1826-1334
HESS J1837-069 (Aharonian et al., 2006a)	PSR J1838-0655

The data was gathered from Imaging Air Cherenkov type Telescope High Energy Stereoscopic System (H.E.S.S.) in 2005 and the Fermi-Large Area Telescope (Fermi-LAT) in 2010 & 2011.

3. THEORY AND METHODOLOGY

3.1 Neutron stars

Neutron stars are the densest and tiniest stars in the universe. They consist of a radius of only about 12-13 km (6 mi), which may have a mass of a few times larger that of the Sun. The neutron stars contain as much mass as 500,000 of earth. These neutron stars appear probably white to the naked eye, although astronomers can workout what is going on beneath their surfaces. The interior structure of a neutron star is shown in Figure 3.1, and the cross-section of a neutron star is shown in Figure 3.2 below.

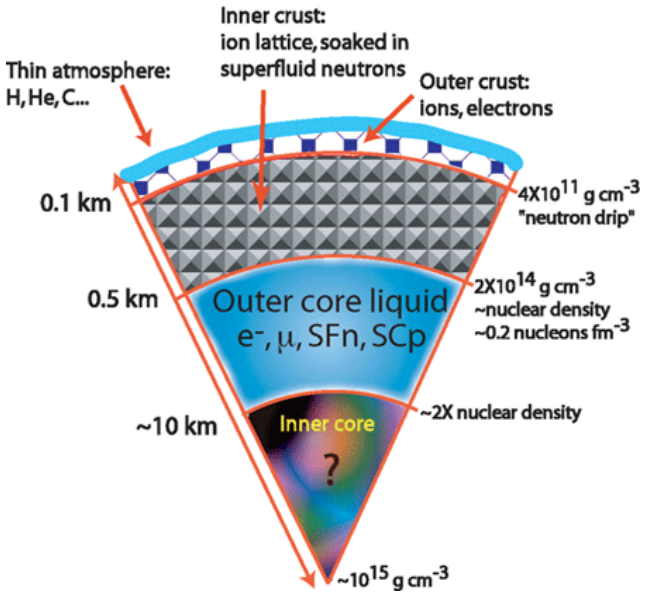

Figure 3.1: Interior structure of the neutron star (Source: www.physics.montana.edu)

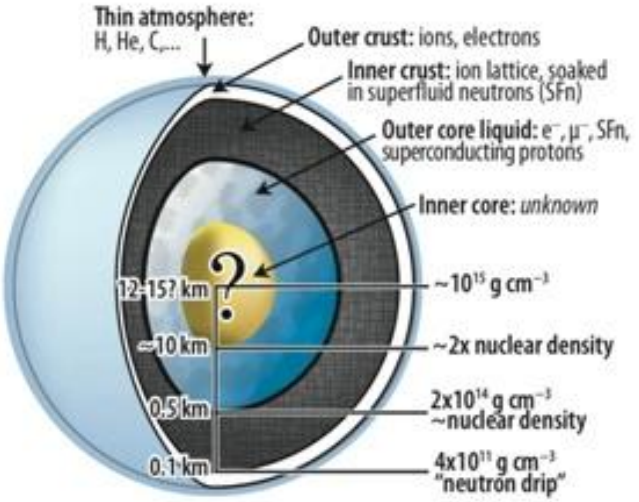

Figure 3.2: Cross-section of the neutron star (Source: heasarc.gsfc.nasa.gov)

Any main sequence star containing a mass around 1.5 to 5 times (**Figure 1.2**) solar masses has the potential to become a neutron star. Neutron stars are very hot and composed almost entirely of neutrons. The surface gravity of a neutron star is about 100 billion times greater than that on earth's surface.

3.2 Pulsars

Someneutron stars have rapid spin and a strong magnetic field. These neutron stars are called Pulsars. Although all pulsars are neutron stars, not all neutron stars are pulsars.

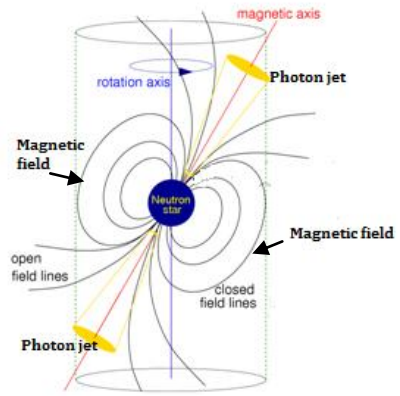

Figure 3.3: Photon jets and magnetic field around the Pulsar (Source: www.4shared.com)

The pulsar works like a dynamo. When the pulsar rotates, the magnetic field surrounding the pulsar gets changed because of the rotational and the magnetic axes of the pulsar are not aligned. Then an electric field is generated with the changes of the magnetic field. Due to the electric field, the electrons on the surface of the pulsar accelerate themselves to high energies. Such accelerated high energy electrons spread around the pulsar as a spiral shape, because of the magnetic field surrounding the pulsar and the angular momentum of the pulsar (Figure 3.3 and Figure 1.4). That is called "**The Pulsar wind**". Also the magnetic field lines shown in Figure 3.3 are converged at the magnetic poles making two cones of **photon jets** outward.The two photon jets and magnetic field around the pulsar is shown in Figure 3.3. These photon jets rotate with the rotation of the pulsar. So, when the rotating photon jets sweep past Earth, it can be detected on the Earth. It's like a beam of light we can see from a lighthouse, when we are in a ship at sea. The Following Figure 3.4 shows this analogy.

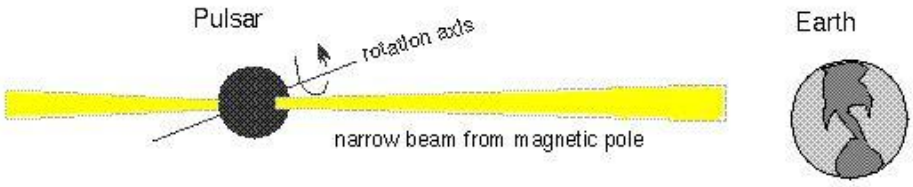

Figure 3.4: Pulsar's Lighthouse analogy (Source: http://www.astronomynotes.com/evolutn/s12.htm)

The energy of the photon jets come from the pulsar's rotational kinetic energy. Therefore the pulsar loses its kinetic energy and slows down, because energy is a constant property. The electron wind produced by the pulsar also makes the pulsar to lose its energy. So the rotating speed of the pulsar slows down because of the electron wind too.

The rate of loss pulsar's rotational kinetic energy is called spin-down luminosity ($\dot{E}$). Spin-down luminosity at a given time can be written as follows:

$$\dot{E}(t) = \dot{E}_o \left(1+\frac{t}{t_o}\right)^{-\left(\frac{n+1}{n-1}\right)} \qquad 3.1$$

Where $\dot{E}_o = \dot{E}\ (t=0)$, t_o is the spin-down timescale and **n** is the braking index. For an ideal pulsar, n=3 from (Manchester & Taylor, 1977). Therefore n=3 was used for relevant calculations.

The spin-down timescale (t_o) is defined by

$$t_o = \frac{2\tau_c}{n-1}\left(\frac{P_o}{P}\right)^{n-1} \qquad 3.2$$

Where

τ_c = Characteristic age of the pulsar

P_o =Initial period of the pulsar

P = Current period of the pulsar

Characteristic age is a rough estimate of the real age of the pulsar. It is defined as,

$$\tau_c = \frac{P}{2\dot{P}} \qquad 3.3$$

Here $\dot{P}$ denotes the time derivative of the rotational period of the Pulsar.

3.3 Pulsar Wind Nebula (PWN)

The pulsar wind generating from the pulsar, takes the form of a cloud, which consists of electrons and positrons. This cloud is called a **Pulsar Wind Nebula (PWN)**. PWN is continuously powered by a relativistic electron/positron wind which comes from its associated pulsar (Figure 3.5).

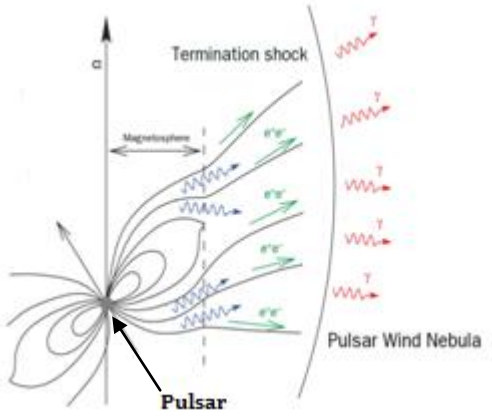

Figure 3.5: 2D diagram of the PWN (Adapted from: www.nature.com)

Crab is a well-known PWN. The following Figure 3.6 shows the visible light and gamma-ray images of the Crab nebula.

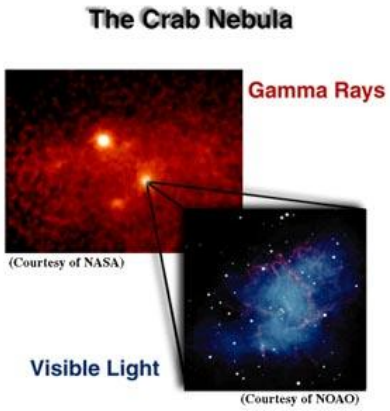

Figure 3.6: Crab nebula (Source: science.hq.nasa.gov)

PWNe form the most abundant class among the galactic sources emitting very high energy gamma-rays. At a distance of about 1000 km from the pulsar, rotational energy of the pulsar is transformed into electromagnetic energy, which in turn is converted to kinetic energy of bulk motion. i.e. acceleration of the wind (Figure 3.7). Finally, the wind terminates by collision with matter (SNRs) in a standing reverse shock about 0.3 light years away from the pulsar (Figure 3.7). That makes a magnetized plasma of relativistic electrons/positrons. This magnetized plasma is usually associated with the non-thermal emissions.

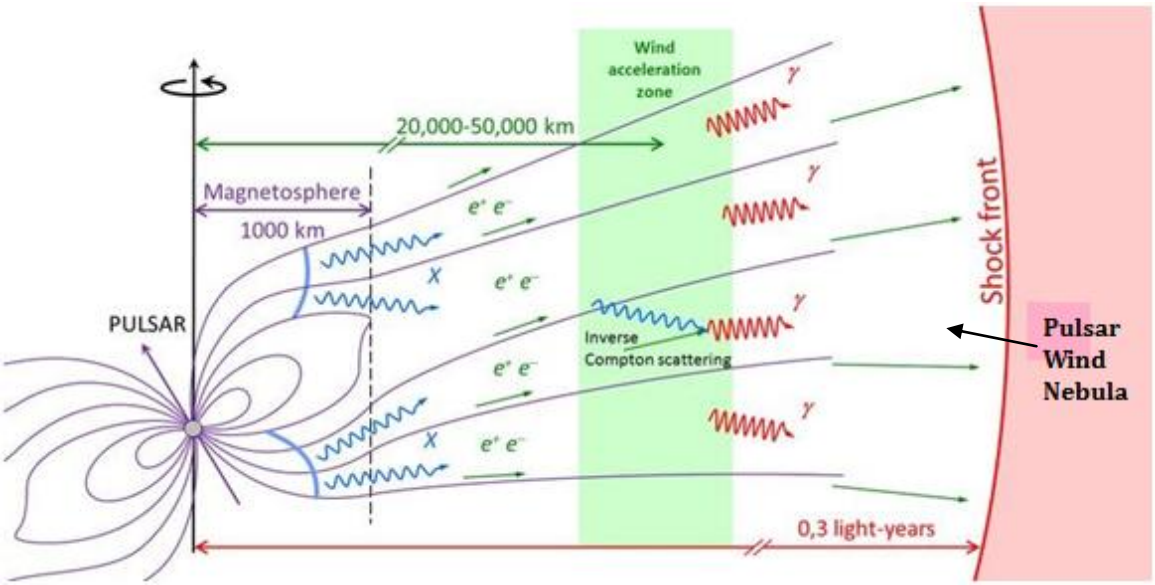

Figure 3.7: Pulsar and Pulsar Wind Nebula system (Source: www.isciencetimes.com)

In the magnetized plasma of relativistic particles, low energy photons can be up scattered by the electrons/positrons to very high energies via the inverse–Compton scattering effect (see Figure 3.7).

3.4 Inverse-Compton scattering and Cooling time

Inverse-Compton scattering associates the scattering of low energy photon to high energies by ultra-relativistic electrons. Therefore photon gain energy and electron lose energy. In other words, the phenomena of inverse-Compton scattering can be described as follows. When an ultra-relativistic electron with Lorentz factor γ collideswith a photon, theresulting collision shift the photon frequency ν roughly to $\gamma^2\nu$, whereby the exact coefficient depends on the (Compton) scattering geometry. The incident of the inverse-Compton effect is shown in Figure 3.8

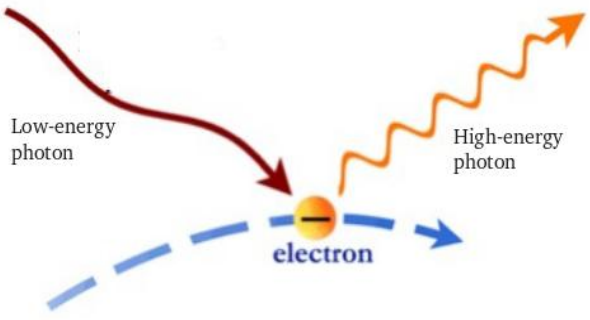

Figure 3.8: Diagram of the inverse-Compton effect (Adapted from: www.thestargarden.co.uk)

The following Figure 3.9 shows the inverse-Compton effect for head-on interaction. (In this study it was assumed that all electrons collide with all photons by the way of head-on interaction)

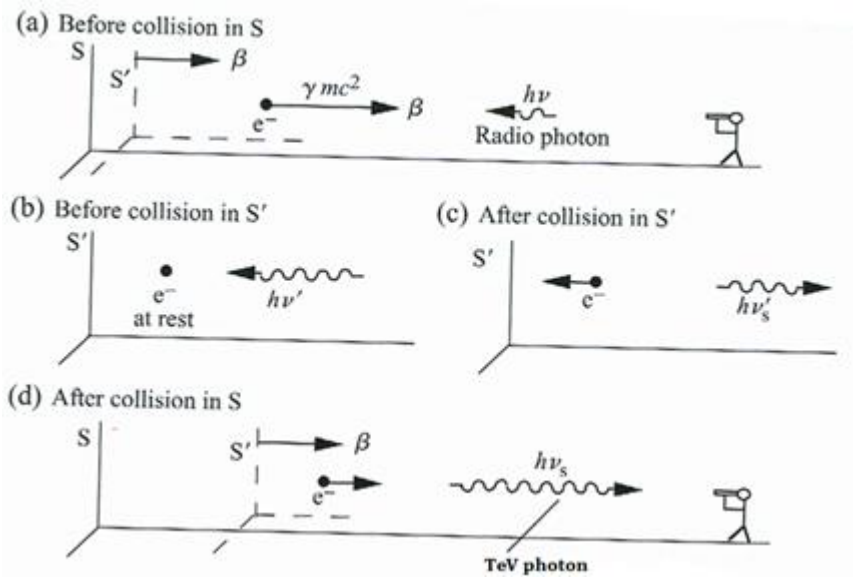

Figure 3.9: Inverse-Compton effect for head-on interaction. (a) **S** frame before the scatter. A highly relativistic electron moves to the right and is about to collide with a left-moving, low-energy (radio) photon of energy hν. The **S′** frame moves with the electron. (b)**S′** frame before scatter. The electron is at rest, and so the scatter becomes a normal Compton scatter. The incident photon in **S′** has been Doppler shifted to higher energy hν′ because of the motion of this frame relative to S. (c) **S′** frame after scatter. The photon, having been backscattered with energy $h\nu'_s$, moves to the right with slightly less energy. (d) **S** frame after scatter. The scattered photon has a much higher energy $h\nu_s >> h\nu'_s$ owing to the transformation back to frame **S**. (Source: http://boojum.as.arizona.edu)

A PWN &its associate pulsar are parts of one system. The PWN is powered by the associated pulsar and pulsar wind generating from the associated pulsar. The high energy electrons in the pulsar wind enter to PWN, in a certain rate. A head on collision with the low energy photon in the PWN was caused by those high energy electrons which entered, resulting in an inverse-Compton scattering phenomena. So, high energy gamma rays emit from the PWN. Because of that high energy gamma rays emit from the PWN, they can be detected using satellites or ground based telescopes on the Earth.

The process happening inside the PWN is equivalent to that of a birth & death process. That means, the entering of an electron to PWN is considered as a birth & the loss of energy of an electron due to the conversion of the high energy electron to low energy electron by inverse-Compton scattering inside the PWN is considered as a death. As the life time in the birth and death process means the time gap between birth and death, the cooling time of ultra-relativistic electrons in PWN means the average time that an ultra-relativistic electron takes to cool-down by inverse-Compton scattering.

3.5 Theory of estimating the cooling time of ultra-relativistic electrons in PWNe

The cooling time means the average time taken by an ultra-relativistic electron to undergo the inverse-Compton scattering process. It is denoted by $T_{cooling}$. The probability of creation of a TeV photon by inverse-Compton scattering of an ultra-relativistic electron in one second can be denoted by $\frac{1}{T_{cooling}}$.

$$\text{inverse-Compton scattering probability} = \frac{1}{T_{cooling}} \quad 3.4$$

In other words, $\frac{1}{T_{cooling}}$ is the inverse scattering frequency, it has the units of per seconds (s^{-1}). This frequency is denoted as "**b**". So the relationship between b & $\frac{1}{T_{cooling}}$ can be written as follows.

$$b = \frac{1}{T_{cooling}} \quad 3.5$$

$$T_{cooling} = \frac{1}{b} \quad 3.6$$

Now, the number of inverse-Compton scattered photons per second can be written as:

$$L_e = b.\ k.\ y \quad 3.7$$

Where **k** is the high energy electron fraction in PWN (# of high energy electrons in PWN **/** Total electrons come from the pulsar), and **y** is the total number of electrons in the PWN at time t.

Then the spin down luminosity of the pulsar can be combined with y and b as follows:

$$\frac{dy}{dt} = \dot{E}_e(t) - b.y \qquad 3.8$$

Where

$\frac{dy}{dt}$ = rate of change of the number electrons exist at time "t" in the PWN

$\dot{E}_e(t)$ = rate of electrons coming in to the PWN

b.y = rate of electrons going out from the PWN

$$\dot{E}_e(t) = \left(\frac{\dot{E}(t)}{\gamma\, m_0 c^2} \right) = \frac{\dot{E}_o t_o^2}{\gamma\, m_0 c^2 .(t + t_o)^2} \qquad 3.9$$

In equation 3.9, $\dot{E}(t)$ is the total energy comes to PWN. It is divided by the energy per electron ($\gamma\, m_0 c^2$) to get the number of electrons come to PWN per second.

$\dot{E}_o$ = initial spin down luminosity of the pulsar

t_o = spin down time scale of the pulsar

γ = bulk Lorentz factor,

m_o = rest mass of the electron=0.511 MeV/c^2 = 0.511 x 10^{-6}TeV/c^2

c = velocity of light

$\gamma\, m_0 c^2 = 0.511 \times 10^{-6} \gamma$ TeV

b = probability that an high energy electron go through inverse-Compton scattering per second (inverse-Compton scattering frequency)

y = number of electrons exist at time t in the PWN

In other words, $\dot{E}_e(t)$ denotes the birth rate and **b.y** denotes the death rate of the process.

The following figure 3.10 shows the block diagram of the PWN & pulsar system in order to understand the concept lying beside the equation 3.8.

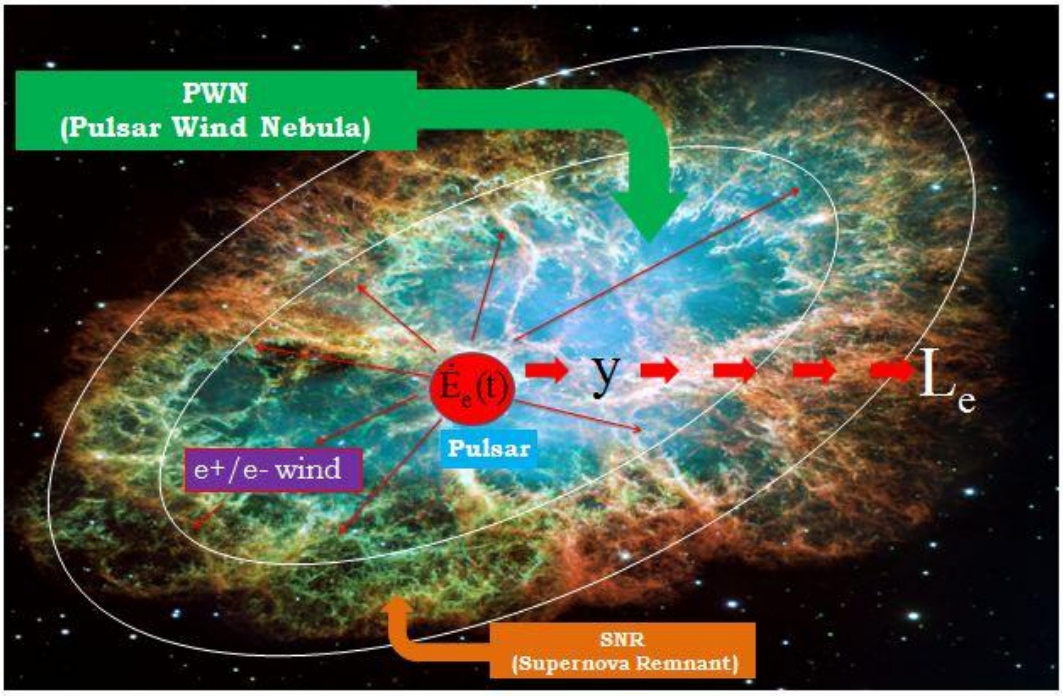

Figure 3.10: Structure of the Pulsar and Pulsar Wind Nebula system (Adapted from: hubblesite.org)

Then the above equation 3.8 can be solved as follows.

$$\frac{dy}{dt} + b.y = \dot{E}_e(t) \qquad 3.10$$

$$I(t)\frac{dy}{dt} + I(t)\,b.y = I(t).\dot{E}_e(t) \qquad 3.11$$

Where I(t)

$$\frac{dI(t)}{dt} = I(t)\,b$$

$$\frac{dI(t)}{I(t)} = b\,dt$$

$$\ln I(t) = b.\,t + C$$

$I(t) = I_o\, e^{bt}$, where I_o is a constant.

Then equation 3.8 becomes as follows.

$$I_o e^{bt}\frac{dy}{dt} + I_o e^{bt} b.\, y = I_o e^{bt}\dot{E}_e(t) \qquad 3.12$$

$$e^{bt}\frac{dy}{dt} + e^{bt} b.\, y = e^{bt}\dot{E}_e(t) \qquad 3.13$$

$$\int_0^{\tau_c} \frac{d[e^{bt} y]}{dt}\, dt = \int_0^{\tau_c} e^{bt}\, \dot{E}_e(t)\, dt \qquad 3.14$$

at t = 0, y = 0

$$y\, e^{b\tau_c} - 0 = \int_0^{\tau_c} e^{bt}\, \dot{E}_e(t)\, dt \qquad 3.15$$

$$y\, e^{b\tau_c} = \int_0^{\tau_c} e^{bt}\, \dot{E}_e(t)\, dt \qquad 3.16$$

$$y\, e^{b\tau_c} = \frac{\dot{E}_o t_o^2}{\gamma m_0 c^2} \int_0^{\tau_c} e^{bt} \frac{1}{(t+t_o)^2}\, dt \qquad 3.17$$

$$y\, e^{b\tau_c} = \frac{\dot{E}_o\, t_o^2}{0.511 \times 10^{-6}\, \gamma} \int_0^{\tau_c} e^{bt} \frac{1}{(t+t_o)^2}\, dt \qquad 3.18$$

$$y = \frac{\dot{E}_o\, t_o^2}{e^{b\tau_c}\, 0.511 \times 10^{-6}\, \gamma} \int_0^{\tau_c} e^{bt} \frac{1}{(t+t_o)^2}\, dt \qquad 3.19$$

Here **y** is not a measurable quantity. However, $L_e$is a measurable parameter. So, both side of the above equation 3.19 were multiplied by **b.k** .

$$y \,.\, b \,.\, k = \frac{b \,.\, k\, \dot{E}_o\, t_o^2}{e^{b\tau_c}\, 0.511 \times 10^{-6}\, \gamma} \int_0^{\tau_c} e^{bt} \frac{1}{(t+t_o)^2}\, dt \qquad 3.20$$

Now this can be rearranged using the equation 3.7.

$$L_e = \frac{b \,.\, k\, \dot{E}_o\, t_o^2}{e^{b\tau_c}\, 0.511 \times 10^{-6}\, \gamma} \int_0^{\tau_c} e^{bt} \frac{1}{(t+t_o)^2}\, dt \qquad 3.21$$

The above equation has 2 unknown parameters except **b**. They are k and γ. Here k is the high energy electron fraction in PWN and γ is the Bulk Lorentz Factor of electrons which are coming from the pulsar wind. The $\dot{E}_o$ and t_o belong to the pulsar properties and L_e belongs to the PWN properties. The exact k and γ values of the four PWNe, which were used in this research, are not estimated yet by any researcher. Therefore the "b" values were found by using a group of k and γ values.

It is not easy to solve the equation 3.21, because it has a complicated integral. So online software, "**Wolfram**. | **Alpha**" was used to solve the equation 3.21. The **Wolfram**. | **Alpha** is an engine for computing answers and it uses its vast store of expert-level knowledge and algorithms to automatically answer questions, do analysis, and generate reports.

Initially, "**b**" values were found for the four PWNe by changing k and γ values and using the equation 3.21. Then the cooling time values were found by using, the obtained "**b**" values and equation 3.6. After that cooling time values were plotted in the k and γ spaces using the MATLAB software. That means, the phase space of the cooling time in k-γ space was found. Finally, ranges for the cooling time of the four PWNe were estimated using the k-γ phase space of the cooling time graphs.

If someone estimates accurately the k and γ values for a PWN, then one can find the "**b**" value from equation 3.21 and then proceed to find the cooling time by applying it to equation 3.6 directly.

3.6 Error Theory

The error of the "b" cannot be found by using the ordinary method (using 1st principles). Because the equation 3.21 has a complicated integral and also "b" is in the complex integral. So the following method was used to find the error value of the "**b**".

$$L_e = \frac{b \,.\, k\, \dot{E}_o\, t_o^2}{e^{b\tau_c}\, 0.511 \times 10^{-6}\, \gamma} \int_0^{\tau_c} e^{bt}\, \frac{1}{(t + t_o)^2}\, dt \qquad 3.22$$

In the above equation 3.22, k and γ are the input parameters of developed model. The error values of the Le, $\dot{E}_o$, $t_o$and τ_c are denoted as δL_e, $\delta \dot{E}_o$, δt_o and $\delta \tau_c$ respectively. The error value of **b**can be found by assuming $\dot{E}_o$, $t_o$and τ_c have no errors and L_e has an error. It is denoted as δL_e. Then obtained **b** values with respect to $\pm L_e$ values are denoted as B_1 and B_2.

$L_e \Rightarrow L_e - \delta L_e$

$b \Rightarrow B_1$

$L_e \Rightarrow L_e + \delta L_e$

$b \Rightarrow B_2$

After that, the above procedure can be applied to $\dot{E}_o$, $t_o$and τ_c as follows.

$\dot{E}_o \Rightarrow \dot{E}_o - \delta\dot{E}_o$
$b \Rightarrow B_3$

$\dot{E}_o \Rightarrow \dot{E}_o + \delta\dot{E}_o$
$b \Rightarrow B_4$

$t_o \Rightarrow t_o - \delta t_o$
$b \Rightarrow B_5$

$t_o \Rightarrow t_o + \delta t_o$
$b \Rightarrow B_6$

$\tau_c \Rightarrow \tau_c - \delta\tau_c$
$b \Rightarrow B_7$

$\tau_c \Rightarrow \tau_c + \delta\tau_c$
$b \Rightarrow B_8$

Then the minus (-) error value and plus (+) error value of the **b** value can be found by using the root mean square value as follows.

$$\text{Minus (-) error value of b} = \sqrt{\frac{\left(b\text{-}B_1\right)^2 + \left(b\text{-}B_3\right)^2 + \left(b\text{-}B_5\right)^2 + \left(b\text{-}B_7\right)^2}{4}}$$

$$\text{Plus (+) error value of b} = \sqrt{\frac{\left(b\text{-}B_2\right)^2 + \left(b\text{-}B_4\right)^2 + \left(b\text{-}B_6\right)^2 + \left(b\text{-}B_8\right)^2}{4}}$$

After that using the equation 3.23 and 3.24, the error value of the cooling time (T) can be found as follows.

$$T_{cooling} = \frac{1}{b} \qquad 3.23$$

$$\left(\frac{\delta T}{T}\right)^2 = \left(\frac{\delta b}{b}\right)^2 \qquad 3.24$$

$$\delta T = \pm T \cdot \left(\frac{\delta b}{b}\right) \qquad 3.25$$

$$\delta T = - T \cdot \left(\frac{\sqrt{\frac{B_1^2 + B_3^2 + B_5^2 + B_7^2}{4}}}{b} \right) \qquad 3.26$$

$$\delta T = + T \cdot \left(\frac{\sqrt{\frac{B_2^2 + B_4^2 + B_6^2 + B_8^2}{4}}}{b} \right) \qquad 3.27$$

4. DATA ANALYSIS AND RESULTS

4.1 Pulsar Properties.

The position of each of four pulsars with coordinates of right ascension and declination are given in Table 4.1 below.

Table 4.1: Position of the four Pulsars

PWNe	Pulsar	Right ascension	Declination
MSH 15-52	PSR B1509-58	$15^h\ 13^m\ 55.52^s$	$-59°\ 08'\ 08.80''$
HESS J1420-607	PSR J1420-6048	$14^h\ 20^m\ 08.20^s$	$-60°\ 48'\ 17.20''$
HESS J1825-137	PSR J1826-1334	$18^h\ 25^m\ 41.00^s$	$-13°\ 50'\ 20.00''$
HESS J1837-069	PSR J1838-0655	$18^h\ 37^m\ 38.40^s$	$-06°\ 57'\ 00.00''$

The rotational period (P) and its time derivative (Ṗ) for all four pulsars were found from the ATNF pulsar database and those values were given in Table 4.2.

Table 4.2: P and Ṗ values of the four Pulsars

PWNe	Pulsar	P (Period) [s]	Ṗ
MSH 15-52	PSR B1509-58	0.15125125831483	1.5314675176E-12
HESS J1420-607	PSR J1420-6048	0.06817987659000	8.3167E-14
HESS J1825-137	PSR J1826-1334	0.10148679420760	7.5251738E-14
HESS J1837-069	PSR J1838-0655	0.07049824396900	4.925E-14

Next, the characteristic ages of the four pulsars were calculated separately using the equation 3.3 in the Theory section. The calculated values are given in Table 4.3.

Table 4.3: Characteristic ages of the four Pulsars

PWNe	Pulsar	τ_c [kyr]
MSH 15-52	PSR B1509-58	1.56
HESS J1420-607	PSR J1420-6048	13.00
HESS J1825-137	PSR J1826-1334	21.40
HESS J1837-069	PSR J1838-0655	22.70

Then the initial period values of above all four pulsars were taken from Mayer et al. 2013; Page 6, TABLE II. The following Table 4.4 shows that the P_o values for all four pulsars.

Table 4.4: Initial period (P_o) values of the four Pulsars

PWNe	Pulsar	P_o[s]
MSH 15-52	PSR B1509-58	0.0389
HESS J1420-607	PSR J1420-6048	0.0332
HESS J1825-137	PSR J1826-1334	0.0260
HESS J1837-069	PSR J1838-0655	0.0307

After that, the spin-down timescale (t_o) values of the four Pulsars were calculated separately using the equation 3.2 in the theory section. The obtained values are given in the Table 4.5.

Table 4.5: Spin-down timescale (t_o) values of the four Pulsars

PWNe	Pulsar	t_o[kyr]
MSH 15-52	PSR B1509-58	0.10
HESS J1420-607	PSR J1420-6048	3.08
HESS J1825-137	PSR J1826-1334	1.40
HESS J1837-069	PSR J1838-0655	4.30

The following Table 4.6 shows that the current rate of loss of rotational kinetic energies (current spin-down luminosity, at t= τ_c) of the four pulsars.

Table 4.6: Current spin-down luminosity values (at t= τ_c) of four Pulsars

PWNe	Pulsar	$\dot{E}$ [s^{-1}TeV]	t=τ_c [kyr]
MSH 15-52	PSR B1509-58	$1.123471682 * 10^{37}$	1.56
HESS J1420-607	PSR J1420-6048	$0.624150934 * 10^{37}$	13.0
HESS J1825-137	PSR J1826-1334	$0.174762261 * 10^{37}$	21.4
HESS J1837-069	PSR J1838-0655	$0.343283013 * 10^{37}$	22.7

Then the initial spin-down luminosity (rate of loss of rotational kinetic energy) values for the four pulsars were calculated using their current rate of spin-down luminosity values. The relationship between the current and initial spin-down luminosity is given in the equation 3.1 in the Theory section. Table 4.7 shows that the calculated initial spin-down luminosities. Here the braking index (n) of all four pulsars was taken as 3.

Table 4.7: Initial spin-down luminosity values (at t=0) of four Pulsars

PWNe	Pulsar	$\dot{E}$ [s^{-1}TeV]	$\dot{E}_o$ [s^{-1}TeV]
MSH 15-52	PSR B1509-58	$1.123471682 * 10^{37}$	$3.095838567*10^{39}$
HESS J1420-607	PSR J1420-6048	$0.624150934 * 10^{37}$	$1.701219220*10^{38}$
HESS J1825-137	PSR J1826-1334	$0.174762261 * 10^{37}$	$4.635123151*10^{38}$
HESS J1837-069	PSR J1838-0655	$0.343283013 * 10^{37}$	$1.353452225*10^{38}$

4.2 Luminosity values of the Pulsar Wind Nebula.

4.2.1 Original SED curves

The following Figure 4.1 shows the Original SED curves of the four PWNe used in this study (Mayer et al., 2013; Page 5, FIG. 3.).

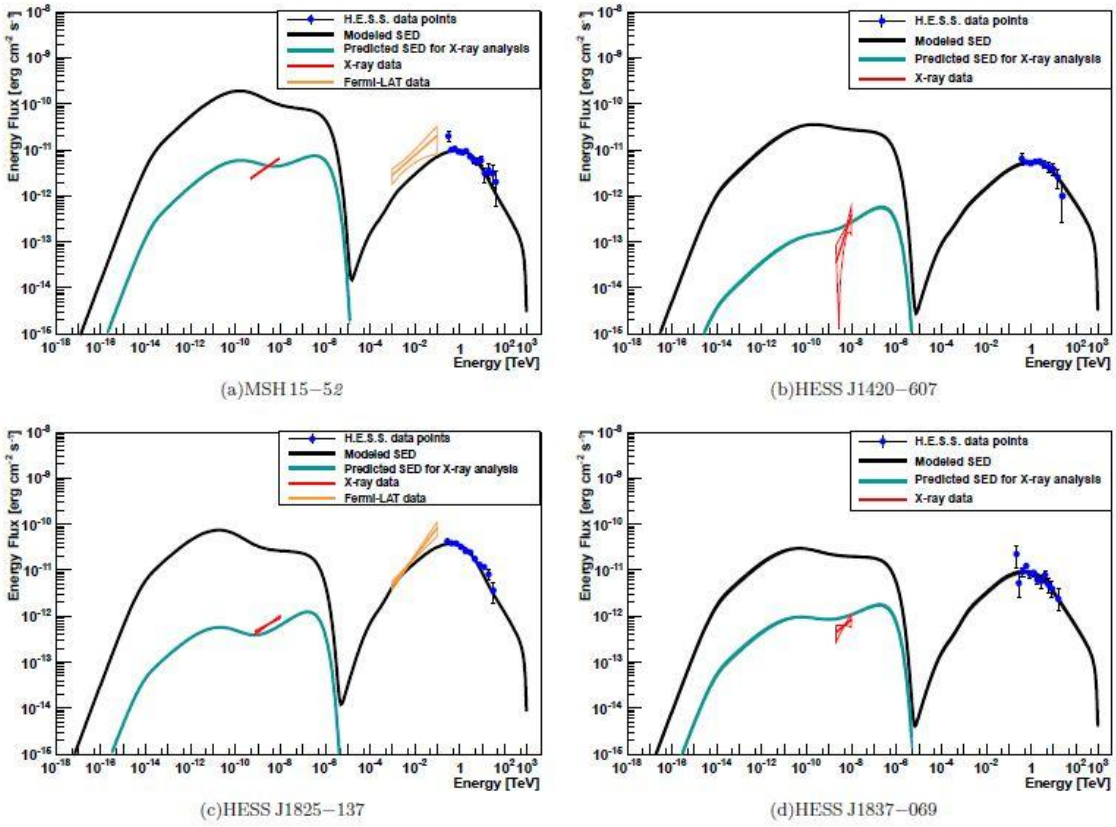

Figure 4.1: Original SED curves of the four PWNe (Source**:** Mayer et al., 2013)

The left side peaks of the above four graphs belong to the synchrotron radiation, which are lying on the x-ray region and the right side peaks belong to the inverse-Compton Scattering phenomenon, within the gamma-ray region. Since this research is dealing only with inverse-Compton scattering phenomenon, the right side peaks of the above all four curves were used. The two axes of the above all four graphs are in log scale.

- X axis = log Energy (TeV)
- Y axis = log Energy flux (erg cm^{-2} s^{-1})

The data of the right side peaks of each graph in Figure 4.1 were obtained by using the Plot Digitizer software. Those data are shown in the Table I in Appendix-I. A screen shot of the plot digitizer software is shown below in Figure 4.2. It shows the way of obtaining data from the original SED curve of MSH 15-52.

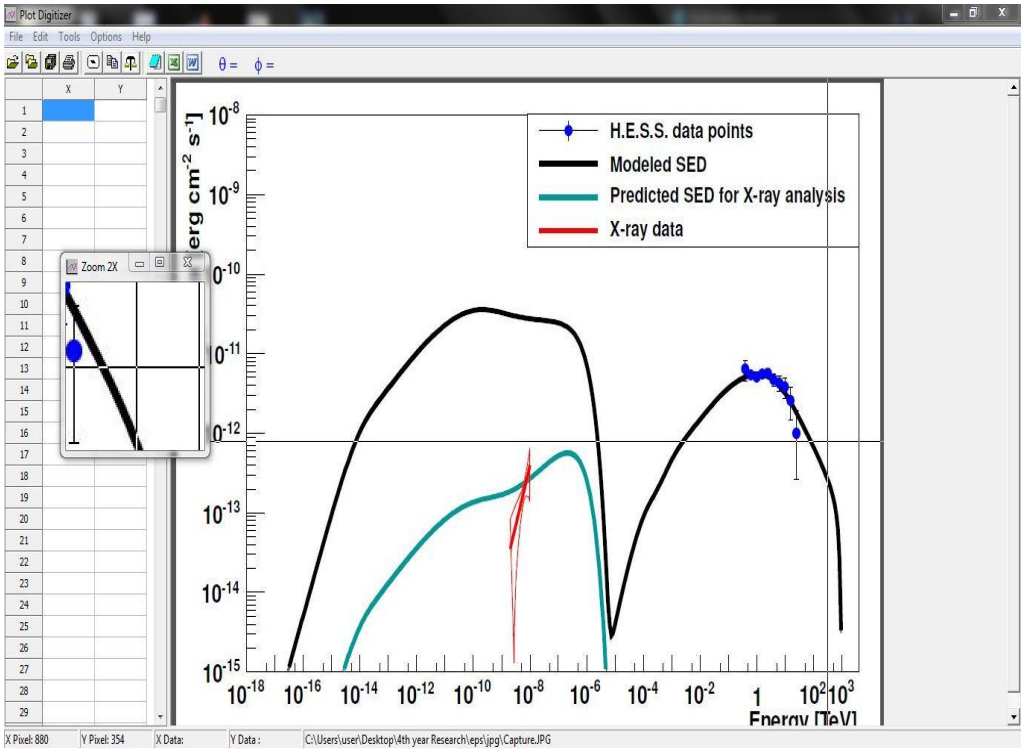

Figure 4.2: Screen shot of the Plot Digitizer software

4.2.2 Fitted SED graphs of the four PWNe

The following fitted curves were plotted using the data obtained in Table I in Appendix-I. Blue color marks show the obtained data points from the original graphs using the plot digitizer software.The fitted function is also given in the top of the every graph. Data denoted by cross marks, was fitted to a 4^{th} order polynomial. Red line in all graphs shows the shape of fitted polynomials in graphically. The **X** axis of each graph in the following Figure 4.3a, Figure 4.3b, Figure 4.3c and Figure 4.3d denotes the energy and its unit is TeV. The **Y** axis of each graph in the following Figure 4.3a, Figure 4.3b, Figure 4.3c and Figure 4.3d denotes the energy flux and its unit is erg cm^{-2} s^{-1}.

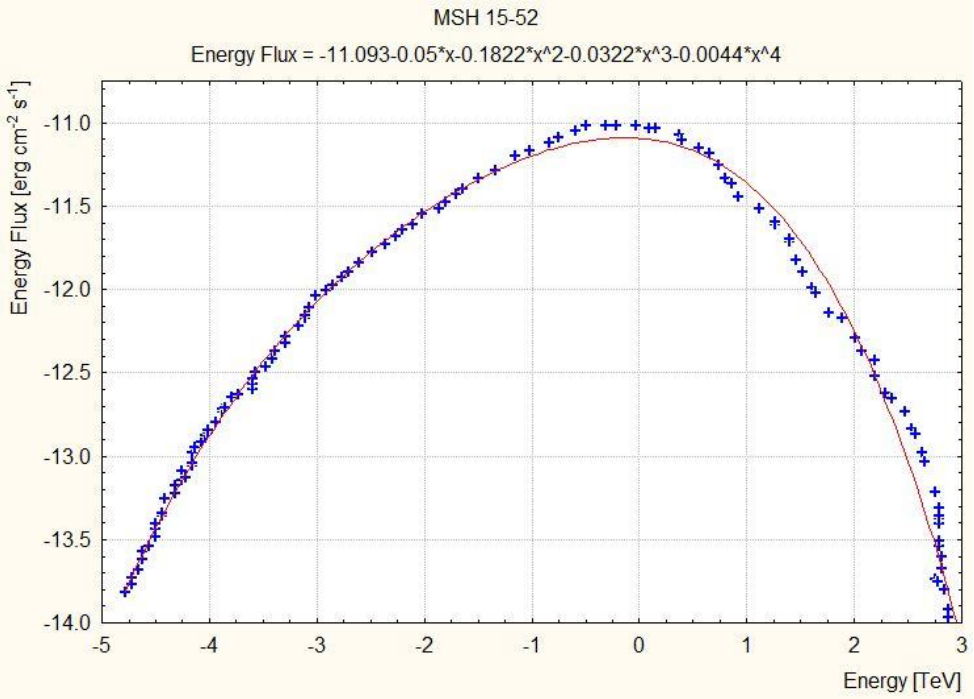

Figure 4.3a: Fitted SED curve for MSH 15-52

This figure shows the best fit curve belonging to original curve in Figure 4.1a.

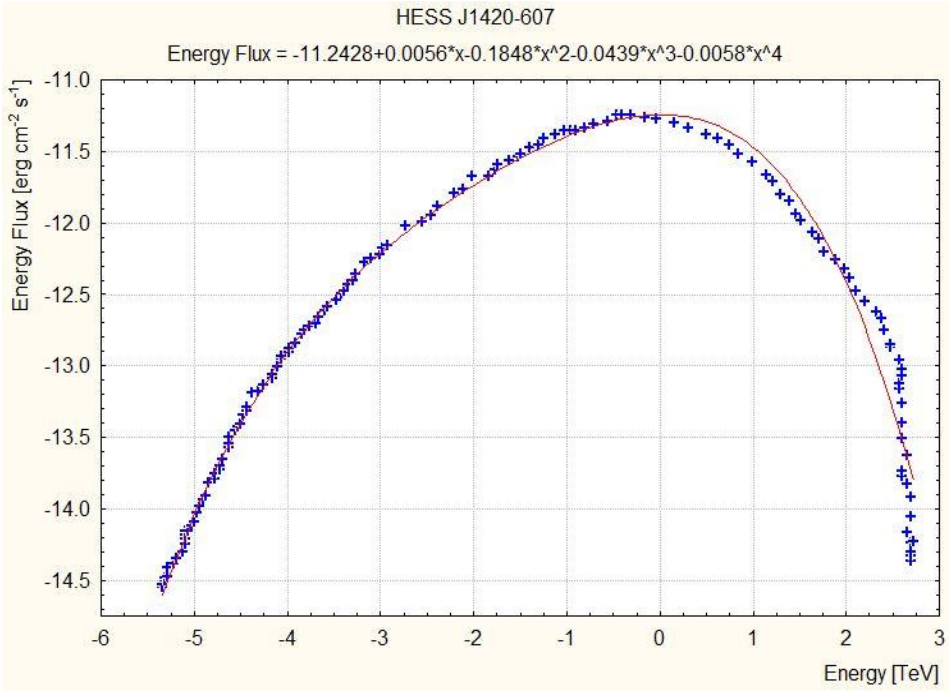

Figure 4.3b: Fitted SED curve for HESS J1420-607

This image shows the best fit curve belonging to original curve in Figure 4.1b.

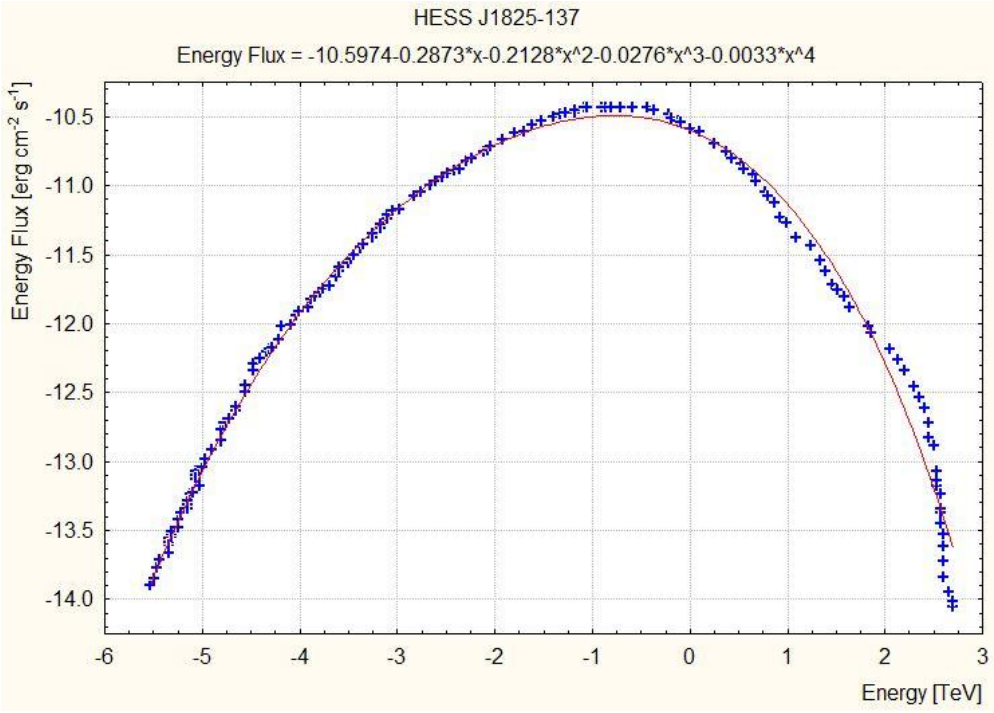

Figure 4.3c: Fitted SED curve for HESS J1825-137

This figure shows the best fit curve belonging to original curve in Figure 4.1c.

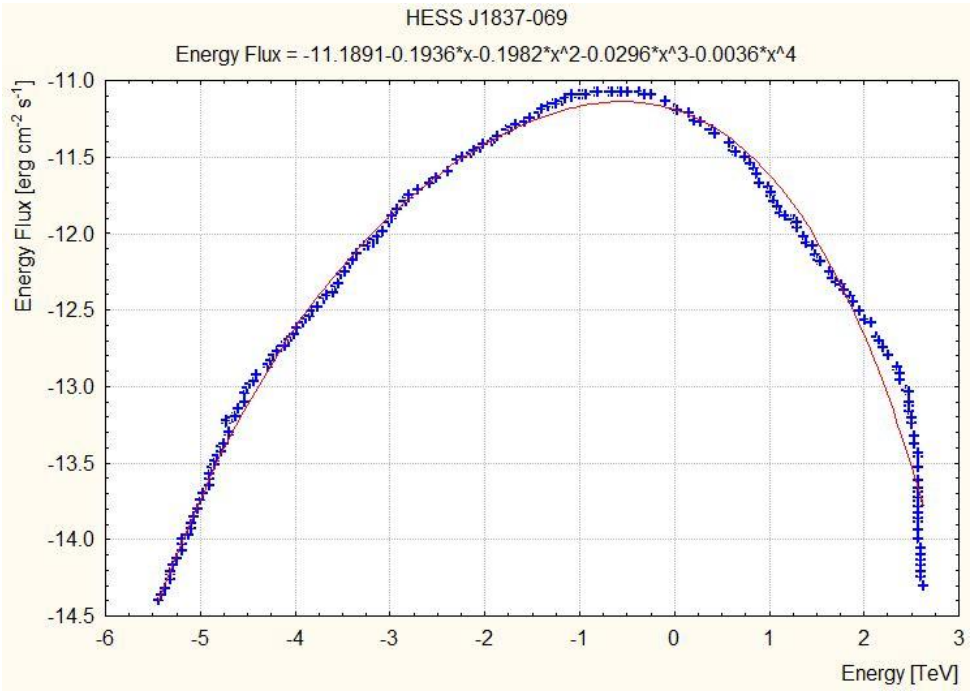

Figure 4.3d: Fitted SED curve for HESS J1837-069

This image shows the best fit curve belonging to original curve in Figure 4.1d.

4.2.3 Photon flux and Luminosity values of the four PWNe

The following Table 4.8 shows the Photon flux values and Luminosity values of the four PWNe. Here photon flux means, the number of photon emitting across $1cm^{-2}$ of the area of the PWN per second (s^{-1}) and luminosity means the number of photon emitting from the whole surface of the PWN per second(s^{-1}).

Table 4.8: Photon flux and Luminosity (L_e) values of the four PWNe

PWNe	D (distance from the erath) [kpc]	[Photon flux] ($cm^{-2}s^{-1}$)	Luminosity(s^{-1}) {L_e values}
MSH 15-52	5.81	$4.063721902 * 10^{-9}$	$1.641320937 * 10^{37}$
HESS J1420-607	7.65	$4.217512693 * 10^{-9}$	$2.953224983 * 10^{37}$
HESS J1825-137	4.12	$41.106580530 * 10^{-9}$	$8.348780603 * 10^{37}$
HESS J1837-069	6.60	$8.573337232 * 10^{-9}$	$4.468430867 * 10^{37}$

4.3 Cooling time values of the four PWNe

The relevant "**b**" values were found using the equation 3.21, t_o values in Table 4.5, $\dot{E}_o$ values in Table 4.7 and L_e values in Table 4.8. In this research, 5 different values of k and γ were used for the four PWNe. Those values are shown in the following Table 4.9 and their ranges are separately shown on the top of each sub table in the Table 4.9. Also the obtained "**b**" values are shown in the Table 4.9 with respect to different k and γ values. The online software, **Wolfram**. | **Alpha** was used to solve the equation 3.21. The screen shot of this software is shown in Figure 4.4. This screen shot shows how to find a "**b**" value of MSH 15-52 with **k = 0.3** and **γ = 5 x 10^5**.

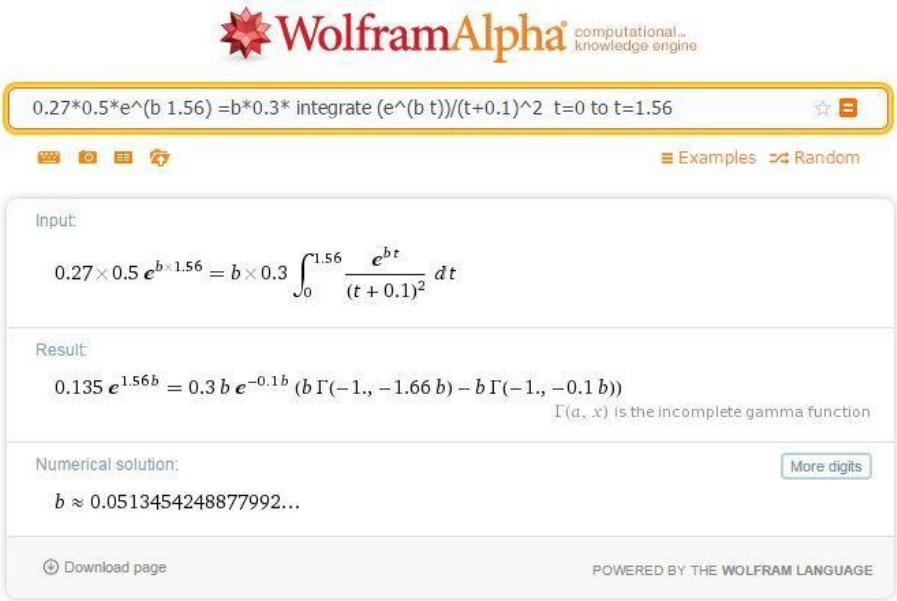

Figure 4.4: Screen shot of the **Wolfram**. | **Alpha** online software

Table 4.9: Data of the **b** values of the four PWNe

(a) MSH 15-52 ($0.1 \leq k \leq 0.9$ **and** $1 \times 10^4 \leq \gamma \leq 1 \times 10^6$)

γ \ k	0.1	0.3	0.5	0.7	0.9
1×10^4	0.002884	0.000958	0.000575	0.000410	0.000319
5×10^4	0.014654	0.004819	0.002884	0.002057	0.001599
1×10^5	0.029924	0.009704	0.005791	0.004127	0.003206
5×10^5	0.184380	0.051345	0.029924	0.021120	0.016319
1×10^6	0.689156	0.111393	0.062558	0.043546	0.033406

(b) HESS J1420-607 ($0.1 \leq k \leq 0.9$ **and** $1 \times 10^3 \leq \gamma \leq 1 \times 10^5$)

γ \ k	0.1	0.3	0.5	0.7	0.9
1×10^3	0.000357	0.000118	0.000071	0.000050	0.000039
5×10^3	0.001812	0.000597	0.000357	0.000255	0.000198
1×10^4	0.003692	0.001201	0.000717	0.000511	0.000397
5×10^4	0.022042	0.006313	0.003692	0.002610	0.002018
1×10^5	0.066935	0.013543	0.007677	0.005362	0.004120

(c) HESS J1825-137 ($0.1 \leq k \leq 0.9$ **and** $5 \times 10^2 \leq \gamma \leq 2.5 \times 10^4$)

γ \ k	0.1	0.3	0.5	0.7	0.9
5.0×10^2	0.000375	0.000124	0.000074	0.000053	0.000041
1.0×10^3	0.000756	0.000249	0.000149	0.000106	0.000082
5.0×10^3	0.004018	0.001272	0.000756	0.000538	0.000417
1.0×10^4	0.008778	0.002609	0.001534	0.001087	0.000841
2.5×10^4	0.036253	0.007090	0.004018	0.002806	0.002156

(d) HESS J1837-069 ($0.1 \leq k \leq 0.9$ **and** $5 \times 10^2 \leq \gamma \leq 5 \times 10^4$)

γ \ k	0.1	0.3	0.5	0.7	0.9
5×10^2	0.000234	0.000077	0.000046	0.000033	0.000025
1×10^3	0.000470	0.000155	0.000093	0.000066	0.000051
5×10^3	0.002434	0.000788	0.000470	0.000335	0.000260
1×10^4	0.005100	0.001599	0.000948	0.000674	0.000523
5×10^4	0.059396	0.009116	0.005100	0.003545	0.002718

Cooling time values of the four PWNe were found in k-γ space by using the obtained '**b**" values. These values were shown in Table 4.10. The unit of the cooling time is kyr.

Table 4.10: Data of the cooling time $\left(\frac{1}{b}\right)$ values of the four PWNe

(a) MSH 15-52 ($0.1 \leq k \leq 0.9$ **and** $1 \times 10^4 \leq \gamma \leq 1 \times 10^6$)

k / γ	0.1	0.3	0.5	0.7	0.9
1×10^4	346.74	1043.84	1739.13	2439.02	3134.79
5×10^4	068.24	0207.51	0346.74	0486.14	0625.39
1×10^5	033.41	0103.05	0172.68	0242.30	0311.91
5×10^5	005.42	0019.47	0033.41	0047.34	0061.27
1×10^6	001.45	0008.97	0015.98	0022.96	0029.93

(b) HESS J1420-607 ($0.1 \leq k \leq 0.9$ **and** $1 \times 10^3 \leq \gamma \leq 1 \times 10^5$)

k / γ	0.1	0.3	0.5	0.7	0.9
1×10^3	2801.12	8474.57	14084.50	20000.00	25641.02
5×10^3	0551.87	1675.04	02801.12	03921.56	05050.50
1×10^4	0270.85	0832.63	01394.70	01956.94	02518.89
5×10^4	0045.36	0158.40	0270.85	00383.14	00495.54
1×10^5	0014.93	0073.83	0130.25	00186.49	00242.71

(c) HESS J1825-137 ($0.1 \leq k \leq 0.9$ **and** $5 \times 10^2 \leq \gamma \leq 2.5 \times 10^4$)

k / γ	0.1	0.3	0.5	0.7	0.9
5.0×10^2	2666.66	8064.51	13513.51	18867.92	24390.24
1.0×10^3	1322.75	4016.06	06711.40	09433.96	12195.12
5.0×10^3	0248.88	0786.16	01322.75	01858.73	02398.08
1.0×10^4	0113.92	0383.28	00651.89	00919.96	01189.06
2.5×10^4	0027.58	0141.04	00248.88	00356.37	00463.82

(d) HESS J1837-069 ($0.1 \leq k \leq 0.9$ **and** $5 \times 10^2 \leq \gamma \leq 5 \times 10^4$)

k / γ	0.1	0.3	0.5	0.7	0.9
5×10^2	4273.50	12987.01	21739.13	30303.03	40000.00
1×10^3	2127.65	06451.61	10752.68	15151.51	19607.84
5×10^3	0410.84	01269.03	02127.65	02985.07	03846.15
1×10^4	0196.07	00625.39	01054.85	01483.67	01912.04
5×10^4	0016.83	00109.69	0196.07	00282.08	00367.91

4.4 k-γ Phase Space of the cooling time of the four PWNe

The following k-γ phase space graphs of cooling time were plotted using the data obtained in Table 4.10 and MATLAB software. In the following graphs (Figure 4.5a, 4.5b, 4.5c, and 4.5d), $T_{cooling}$ means the cooling time with unit of kyr and cooling time values are illustrated using coloured squares. The color bar on the right side of each graph indicates the corresponding $T_{cooling}$ value for each color. The **X** axis of each graph in the following Figure 4.5a, Figure 4.5b, Figure 4.5c and Figure 4.5d is the Bulk Lorentz factor (γ) of electrons in the PWN. The **Y** axis of each graph in the following Figure 4.5a, Figure 4.5b, Figure 4.5c and Figure 4.5d is the high energy electron fraction (k) in PWN. Also **Z** axis (color squares) is the cooling time ($T_{cooling}$). The white color in every plot (Figure 4.5) indicates the region of $T_{cooling} < 0$. Time cannot be a negative value. Therefore, this region gives the forbidden space for k and γ.

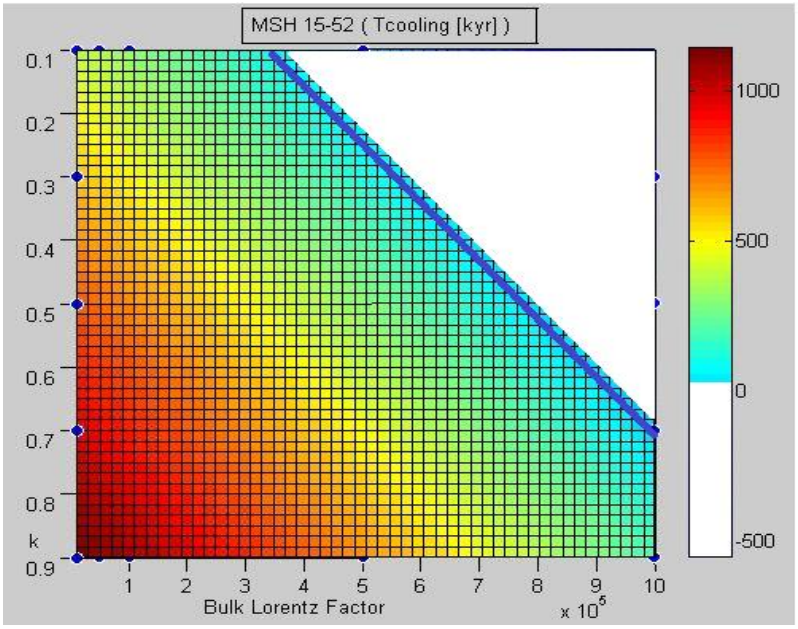

Figure 4.5a: k-γ phase space of the cooling time for MSH 15-52

This is the k-γ phase space of the cooling time for MSH 15-52. Here blue color line shows the characteristic age of the associated pulsar (PSR B1509-58). It is equal to 1.56 kyr.

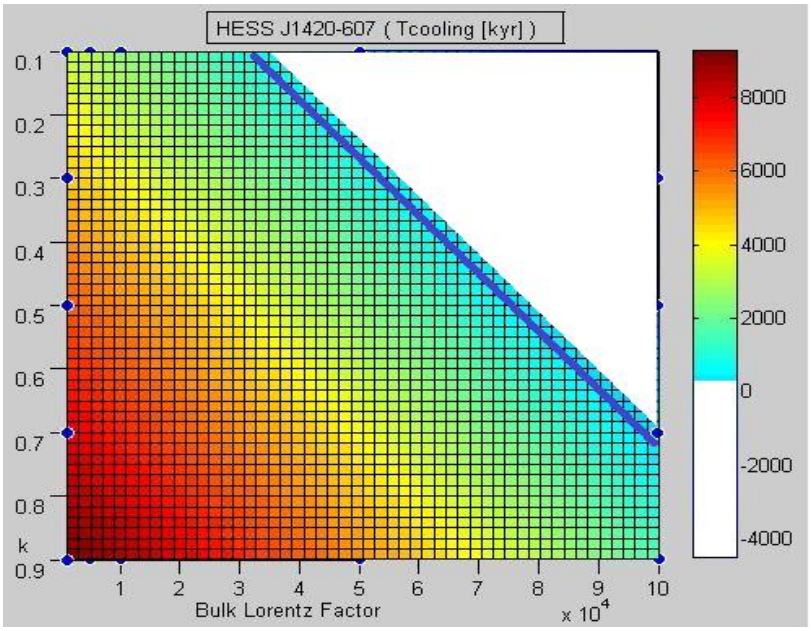

Figure 4.5b: k-γ phase space of the cooling time for HESS J1420-607

This is the k-γ phase space of the cooling time for HESS J1420-607. Here blue color line shows the characteristic age of the associated pulsar (PSR J1420-6048). It is equal to 13.0 kyr.

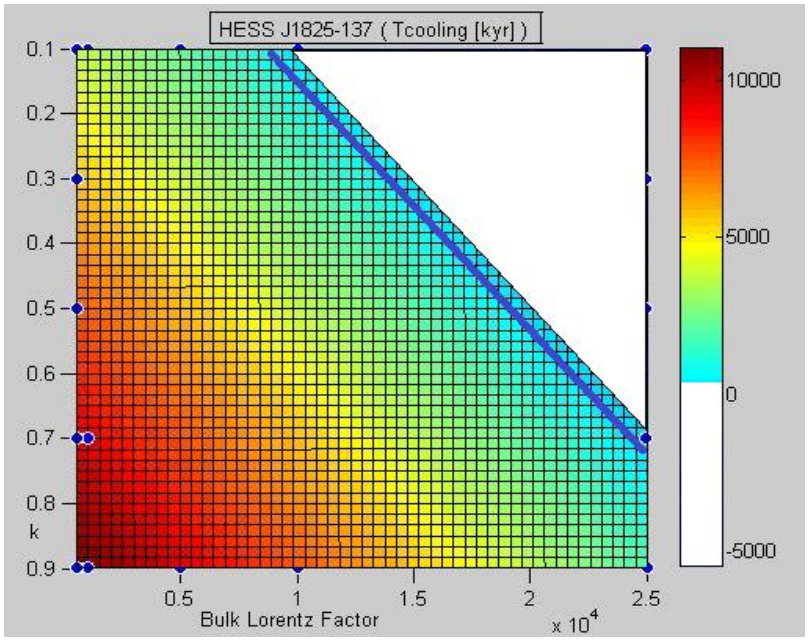

Figure 4.5c: k-γ phase space of the cooling time for HESS J1825-137

This is the k-γ phase space of the cooling time for HESS J1825-137. Here blue color line shows the characteristic age of the associated pulsar (PSR J1826-1334). It is equal to 21.4 kyr.

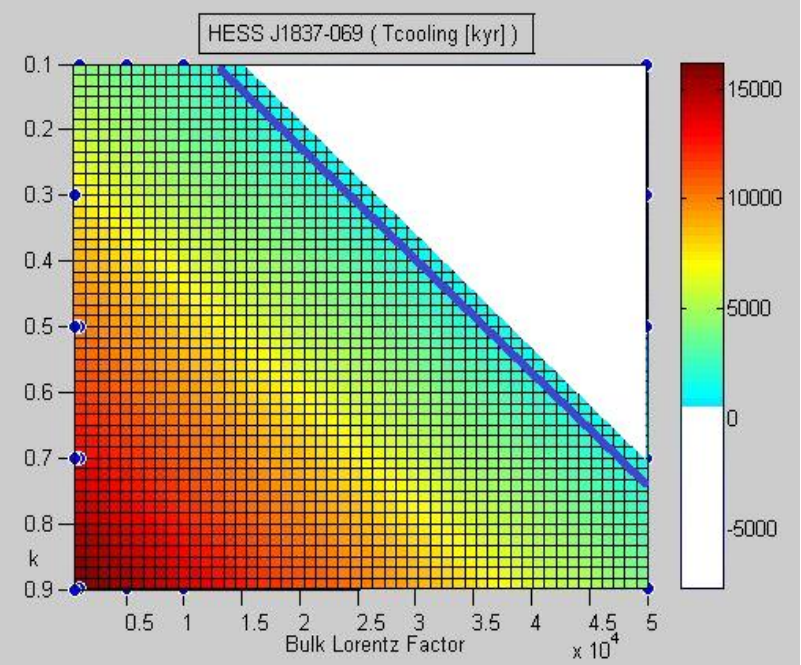

Figure 4.5d: k-γ phase space of the cooling time for HESS J1837-069

This is the k-γ phase space of the cooling time for HESS J1837-069. Here blue color line shows the characteristic age of the associated pulsar (PSR J1838-0655). It is equal to 22.7 kyr.

The cooling time of ultra-relativistic electrons in the PWNe should be more than the characteristic age of the associated Pulsar of the PWN (Mattana et al., 2009). Using the k-γ phase space of the cooling time, ranges which consist the possible numerical values for the cooling time of four PWNe were estimated (Table 4.11).

Table 4.11: Ranges of the cooling time vary of the four PWNe

PWNe	**Ranges of the cooling time varies [kyr]**	**Ranges of the k varies**	**Ranges of the γ varies**
MSH 15-52	01.56 - 1000	0.1 – 0.9	$1 \times 10^4 – 1.0 \times 10^6$
HESS J1420-607	13.00 - 8000	0.1 – 0.9	$1 \times 10^3 – 1.0 \times 10^5$
HESS J1825-137	21.40 - 10000	0.1 – 0.9	$5 \times 10^2 – 2.5 \times 10^4$
HESS J1837-069	22.70 - 15000	0.1 – 0.9	$5 \times 10^2 – 5.0 \times 10^4$

4.5 Error Calculations

The relevant error calculation of the **b** value and the cooling time (T) value are given below. This error calculation belongs to MSH 15-52 with **k = 0.3** and **$\gamma = 5 \times 10^5$**.

Minus (-) error value of b $= \sqrt{\frac{(b-B_1)^2 + (b-B_3)^2 + (b-B_5)^2 + (b-B_7)^2}{4}} = 0.048809$

Plus (+) error value of b $= \sqrt{\frac{(b-B_2)^2 + (b-B_4)^2 + (b-B_6)^2 + (b-B_8)^2}{4}} = 0.052197$

For MSH 15-52,

When k = 0.3 and $\gamma = 5 \times 10^5$

b = 0.051345

T = 19.47 kyr

So the error values of the cooling time (T) of MSH 15-52, when k = 0.3 and $\gamma = 5 \times 10^5$ are given below.

$\delta T = -18.50$ kyr

$\delta T = +19.79$ kyr

5. DISCUSSION

This thesis invented a novel statistical method to estimate the cooling time of ultra-relativistic electrons in PWNe using PWN's gamma ray luminosity, period and spin-down luminosity of the associated pulsar. The developed statistical method is a model independent method. It can be applied to any PWN with a detectable pulsar. Therefore one can find the cooling time easily using this method. This is the main advantage of this new statistical method developed during study.

The luminosity values of the four PWNe were found by fitting the obtained data to the 4^{th} order polynomial. The original SED curves were plotted by taking the data from the H.E.S.S. and Fermi-LAT telescopes. Those original SED curves have few data points because of the limited detecting energy range of the current instruments.

The cooling time was found to be depending on k and γ values. The exact k and γ values for the four PWNe used here are not estimated yet by any researcher. As such, values within a particular range for k and γ were used. Here k is a fraction which should lie between zero and one. Five different k values were used (k = 0.1, 0.3, 0.5, 0.7, 0.9) for all four PWNe. However, one can use any value for k, but it should be in the range between zero and one because k is fraction. Also one can use more than five values for k. If someone estimates the exact value for **k** for a PWN then that value can be applied directly for k.

Four different ranges of γ values were used due to the fact that γ depends on the characteristic age of the associated pulsar of the PWN. So the γ value of a PWN, with less characteristic age of the associated pulsar has a high value (e.g. MSH 15-52) and with high characteristic age of the associated pulsar has a less value (e.g. HESS J1837-069).

Cooling time of a PWN should be in the kyr (1000 years) scale (Mattana, 2009) and the estimated ranges for cooling time of all four selected PWNe are also in the kyr scale (Table 4.11).

6. CONCLUSIONS

A novel statistical method was successfully developed to estimate the inverse-Compton scattering cooling time of a PWN using the properties of the PWN and its associated pulsar. The developed method is a model independent technique. It can be applied to any PWN with a detectable pulsar.

Cooling time depends on two parameters: k and $\boldsymbol{\gamma}$. Here k means high energy electron fraction in PWN and $\boldsymbol{\gamma}$ means Bulk Lorentz Factor of electrons in PWN. The k-$\boldsymbol{\gamma}$ phase space of the cooing time was found for four selected PWNe. Cooling time is proportional to k and it is inversely proportional to γ. Ranges which consist the possible numerical values for the cooling time of four PWNe were estimated (Table 4.11) using the k-γ phase space of the cooling time. Cooling time of a PWN should be in the kyr scale and the estimated ranges for cooling time of all four selected PWNe are also in the kyr scale (Table 4.11).

Appendix-I Data set from SED curves of four PWNe

The following Table I shows the data, obtained from original SED curves of four PWNe, using plot digitizer software.

Table I: Data set from SED curves of four PWNe

MSH 15-52		**HESS J1420-607**		**HESS J1825-137**		**HESS J1837-069**	
Energy [Tev]	**Energy Flux** [erg cm^{-2} s^{-1}]	**Energy** [Tev]	**Energy Flux** [erg cm^{-2} s^{-1}]	**Energy** [Tev]	**Energy Flux** [erg cm^{-2} s^{-1}]	**Energy** [Tev]	**Energy Flux** [erg cm^{-2} s^{-1}]
-4.7825	-13.8173	-5.34235	-14.5479	-5.52705	-13.8938	-5.43507	-14.3958
-4.72037	-13.7716	-5.34235	-14.5479	-5.49593	-13.8481	-5.40399	-14.3654
-4.72027	-13.726	-5.34232	-14.5327	-5.46475	-13.772	-5.37288	-14.3197
-4.65814	-13.6803	-5.31124	-14.5023	-5.43361	-13.7111	-5.31071	-14.2588
-4.62699	-13.6194	-5.3112	-14.487	-5.43361	-13.7111	-5.31065	-14.2284
-4.6269	-13.5738	-5.28015	-14.4718	-5.34046	-13.6654	-5.31062	-14.2132
-4.5648	-13.5433	-5.28002	-14.411	-5.34036	-13.6198	-5.2795	-14.1675
-4.50264	-13.4824	-5.28002	-14.411	-5.34033	-13.6046	-5.24839	-14.1219
-4.50254	-13.4368	-5.21793	-14.3805	-5.34033	-13.6046	-5.18626	-14.0762
-4.50247	-13.4063	-5.18684	-14.35	-5.34033	-13.6046	-5.18616	-14.0305
-4.44034	-13.3607	-5.18684	-14.35	-5.3403	-13.5894	-5.1861	-14.0001
-4.44031	-13.3455	-5.12472	-14.3044	-5.34023	-13.5589	-5.124	-13.9696
-4.4091	-13.2541	-5.12472	-14.3044	-5.30918	-13.5437	-5.09289	-13.924
-4.31599	-13.2237	-5.09357	-14.2435	-5.30918	-13.5437	-5.09289	-13.924
-4.31589	-13.178	-5.0935	-14.2131	-5.30918	-13.5437	-5.09282	-13.8935
-4.25379	-13.1476	-5.09344	-14.1826	-5.30915	-13.5285	-5.09282	-13.8935
-4.25366	-13.0867	-5.09337	-14.1522	-5.30912	-13.5133	-5.06171	-13.8479
-4.22274	-13.1323	-5.06236	-14.1522	-5.30912	-13.5133	-5.03059	-13.8022
-4.16055	-13.0562	-5.06236	-14.1522	-5.30912	-13.5133	-4.99945	-13.7413
-4.16052	-13.041	-5.03128	-14.1217	-5.24702	-13.4828	-4.96837	-13.7109
-4.16039	-12.9801	-5.0002	-14.0913	-5.24689	-13.422	-4.96833	-13.6957
-4.1293	-12.9497	-4.96905	-14.0304	-5.21578	-13.3763	-4.9062	-13.65
-4.06721	-12.9192	-4.93793	-13.9848	-5.15368	-13.3458	-4.90611	-13.6044
-4.03609	-12.8736	-4.90682	-13.9391	-5.15362	-13.3154	-4.90604	-13.5739
-4.00504	-12.8583	-4.90682	-13.9391	-5.15355	-13.285	-4.87493	-13.5283
-4.00501	-12.8431	-4.87574	-13.9086	-5.15355	-13.285	-4.84388	-13.513
-3.94288	-12.7975	-4.84453	-13.8173	-5.12244	-13.2393	-4.84381	-13.4826
-3.94288	-12.7975	-4.78243	-13.7869	-5.09139	-13.2241	-4.81273	-13.4522
-3.88072	-12.7366	-4.78243	-13.7869	-5.06018	-13.1328	-4.78165	-13.4217
-3.88069	-12.7213	-4.78237	-13.7564	-5.06011	-13.1023	-4.78159	-13.3913
-3.84964	-12.7061	-4.72027	-13.726	-5.06005	-13.0719	-4.75054	-13.376
-3.78748	-12.6452	-4.72027	-13.726	-5.02926	-13.1784	-4.71923	-13.2391
-3.72541	-12.63	-4.72021	-13.6956	-5.029	-13.0567	-4.7192	-13.2239
-3.60128	-12.5995	-4.68909	-13.6499	-4.99795	-13.0414	-4.68838	-13.3152
-3.60122	-12.569	-4.6269	-13.5738	-4.96684	-12.9958	-4.68834	-13.2999

-3.60115	-12.5386	-4.6269	-13.5738	-4.96684	-12.9958	-4.65713	-13.2086
-3.57004	-12.493	-4.62683	-13.5434	-4.9668	-12.9806	-4.62608	-13.1934
-3.47692	-12.4625	-4.62673	-13.4977	-4.9668	-12.9806	-4.59497	-13.1477
-3.4148	-12.4168	-4.5646	-13.452	-4.90464	-12.9197	-4.53284	-13.1021
-3.38368	-12.3711	-4.53352	-13.4216	-4.81146	-12.8588	-4.53271	-13.0412
-3.29054	-12.3254	-4.50247	-13.4063	-4.81143	-12.8436	-4.53271	-13.0412
-3.29044	-12.2798	-4.47133	-13.3455	-4.81127	-12.7675	-4.50163	-13.0108
-3.16624	-12.2189	-4.44025	-13.315	-4.81127	-12.7675	-4.47055	-12.9803
-3.10411	-12.1732	-4.44025	-13.315	-4.78015	-12.7218	-4.4395	-12.9651
-3.10408	-12.158	-4.44018	-13.2846	-4.78015	-12.7218	-4.40838	-12.9194
-3.07297	-12.1123	-4.37795	-13.1933	-4.74914	-12.7218	-4.28422	-12.8737
-3.01077	-12.0362	-4.31589	-13.178	-4.71806	-12.6914	-4.28419	-12.8585
-2.91766	-12.0057	-4.31589	-13.178	-4.65589	-12.6305	-4.25311	-12.828
-2.85556	-11.9753	-4.25376	-13.1323	-4.65589	-12.6305	-4.22203	-12.7976
-2.76242	-11.9296	-4.16061	-13.0867	-4.65583	-12.6	-4.19095	-12.7672
-2.70032	-11.8991	-4.16061	-13.0867	-4.56255	-12.4935	-4.12885	-12.7367
-2.60714	-11.8382	-4.16055	-13.0562	-4.56246	-12.4478	-4.09783	-12.7367
-2.48295	-11.7773	-4.09842	-13.0105	-4.46918	-12.3413	-4.06672	-12.691
-2.35878	-11.7316	-4.09842	-13.0105	-4.46908	-12.2956	-4.03567	-12.6758
-2.26564	-11.6859	-4.06727	-12.9497	-4.40695	-12.25	-4.00462	-12.6605
-2.20351	-11.6402	-4.06724	-12.9345	-4.34482	-12.2043	-3.97351	-12.6149
-2.1104	-11.6097	-3.97413	-12.904	-4.31377	-12.189	-3.97351	-12.6149
-2.01722	-11.5488	-3.97406	-12.8735	-4.28272	-12.1738	-3.91141	-12.5844
-1.86207	-11.5183	-3.91196	-12.8431	-4.22056	-12.1129	-3.88033	-12.554
-1.79994	-11.4726	-3.8498	-12.7822	-4.18935	-12.0216	-3.84928	-12.5387
-1.7068	-11.4269	-3.81872	-12.7517	-4.18935	-12.0216	-3.8182	-12.5083
-1.6447	-11.3965	-3.75662	-12.7213	-4.09627	-12.0063	-3.7561	-12.4778
-1.48949	-11.3355	-3.69456	-12.706	-4.03411	-11.9455	-3.69397	-12.4322
-1.33431	-11.2898	-3.66344	-12.6604	-4.00303	-11.915	-3.69394	-12.4169
-1.14802	-11.1984	-3.60132	-12.6147	-3.90991	-11.8845	-3.66289	-12.4017
-1.02389	-11.1679	-3.57023	-12.5842	-3.87877	-11.8237	-3.60083	-12.3865
-0.8377	-11.1222	-3.47709	-12.5386	-3.87877	-11.8237	-3.56971	-12.3408
-0.74458	-11.0917	-3.41496	-12.4929	-3.84772	-11.8084	-3.53866	-12.3256
-0.5894	-11.046	-3.38391	-12.4776	-3.78562	-11.778	-3.50752	-12.2647
-0.49629	-11.0155	-3.3528	-12.432	-3.75454	-11.7475	-3.47647	-12.2495
-0.31019	-11.0154	-3.2907	-12.4015	-3.69248	-11.7323	-3.41434	-12.2038
-0.21714	-11.0153	-3.25958	-12.3559	-3.63028	-11.6562	-3.38326	-12.1733
-0.03105	-11.0152	-3.16637	-12.2797	-3.5992	-11.6257	-3.35214	-12.1277
0.092984	-11.0304	-3.10428	-12.2493	-3.5992	-11.6257	-3.259	-12.082
0.155014	-11.0303	-3.01116	-12.2188	-3.59913	-11.5953	-3.22798	-12.082
0.37203	-11.0759	-2.98005	-12.1731	-3.50602	-11.5648	-3.16592	-12.0667
0.402981	-11.1063	-2.91798	-12.1579	-3.47494	-11.5344	-3.16585	-12.0363
0.557964	-11.1519	-2.7316	-12.0208	-3.44386	-11.5039	-3.1348	-12.0211
0.650947	-11.1822	-2.54543	-11.9903	-3.38173	-11.4582	-3.07271	-11.9906
0.743833	-11.2583	-2.45229	-11.9446	-3.38173	-11.4582	-3.01054	-11.9297
0.805702	-11.3343	-2.39013	-11.8837	-3.3817	-11.443	-3.01054	-11.9297

0.867669	-11.3647	-2.20383	-11.7923	-3.35065	-11.4278	-2.97946	-11.8993
0.929538	-11.4408	-2.11072	-11.7619	-3.2575	-11.3821	-2.97943	-11.884
1.115471	-11.5167	-2.01748	-11.6705	-3.25744	-11.3517	-2.9173	-11.8384
1.270357	-11.6079	-1.83138	-11.6704	-3.16429	-11.306	-2.85517	-11.7927
1.27039	-11.5927	-1.76925	-11.6247	-3.16423	-11.2755	-2.85517	-11.7927
1.394194	-11.7144	-1.73817	-11.5943	-3.16423	-11.2755	-2.85517	-11.7927
1.394226	-11.6992	-1.61404	-11.5638	-3.10213	-11.2451	-2.82415	-11.7927
1.455998	-11.8209	-1.52093	-11.5333	-3.10206	-11.2146	-2.82415	-11.7927
1.517867	-11.8969	-1.48988	-11.5181	-3.03997	-11.1842	-2.79307	-11.7622
1.610721	-11.9881	-1.39673	-11.4724	-2.9779	-11.1689	-2.79304	-11.747
1.641671	-12.0186	-1.39673	-11.4724	-2.82263	-11.0776	-2.69993	-11.7165
1.765476	-12.1402	-1.30365	-11.4571	-2.76053	-11.0471	-2.57577	-11.6708
1.889475	-12.1706	-1.24152	-11.4115	-2.66738	-11.0014	-2.51367	-11.6404
2.01328	-12.2922	-1.11739	-11.381	-2.66738	-11.0014	-2.38951	-11.5946
2.075149	-12.3683	-1.02428	-11.3505	-2.60529	-10.9709	-2.2963	-11.5185
2.198888	-12.5204	-0.96225	-11.3505	-2.54319	-10.9405	-2.23423	-11.5033
2.199083	-12.4291	-0.90022	-11.3504	-2.48109	-10.91	-2.14112	-11.4728
2.291708	-12.6268	-0.80713	-11.3352	-2.41903	-10.8948	-2.11007	-11.4576
2.353674	-12.6572	-0.71402	-11.3047	-2.35696	-10.8795	-2.048	-11.4423
2.477576	-12.7332	-0.55891	-11.2894	-2.2948	-10.8186	-2.01692	-11.4119
2.53938	-12.8397	-0.46576	-11.2437	-2.23273	-10.8034	-1.92384	-11.3966
2.570332	-12.8701	-0.40373	-11.2437	-2.10857	-10.7577	-1.92384	-11.3966
2.632135	-12.9766	-0.31068	-11.2436	-2.07752	-10.7424	-1.89279	-11.3814
2.663021	-13.0374	-0.15563	-11.2587	-2.04644	-10.712	-1.86174	-11.3661
		-0.0316	-11.2739	-1.92228	-10.6663	-1.7686	-11.3204
		0.15443	-11.3042	-1.79812	-10.6206	-1.73758	-11.3204
		0.309445	-11.3346	-1.70504	-10.6053	-1.70654	-11.3052
		0.495443	-11.3801	-1.61189	-10.5596	-1.67549	-11.29
		0.619443	-11.4105	-1.51878	-10.5291	-1.58241	-11.2747
		0.743409	-11.4561	-1.39465	-10.4986	-1.52031	-11.2442
		0.836327	-11.5169	-1.33258	-10.4834	-1.4272	-11.2138
		0.991278	-11.5777	-1.27052	-10.4681	-1.39611	-11.1833
		1.146162	-11.6689	-1.17747	-10.4681	-1.33405	-11.1681
		1.208097	-11.7145	-1.17744	-10.4529	-1.27198	-11.1528
		1.30095	-11.8057	-1.08436	-10.4376	-1.24097	-11.1528
		1.393901	-11.8513	-1.05334	-10.4376	-1.1789	-11.1376
		1.455738	-11.9426	-0.89826	-10.4375	-1.14786	-11.1223
		1.517672	-11.9882	-0.86725	-10.4375	-1.08579	-11.1071
		1.641574	-12.0642	-0.80521	-10.4375	-1.08576	-11.0919
		1.703508	-12.1098	-0.71216	-10.4374	-0.99271	-11.0918
		1.765345	-12.2011	-0.5881	-10.4373	-0.96169	-11.0918
		1.889279	-12.2619	-0.43302	-10.4373	-0.93068	-11.0918
		1.982197	-12.3227	-0.37102	-10.4525	-0.8376	-11.0765
		2.044101	-12.3835	-0.21601	-10.4828	-0.80658	-11.0765
		2.105936	-12.4748	-0.18505	-10.5132	-0.68252	-11.0764
		2.198822	-12.5508	-0.12306	-10.5284	-0.6515	-11.0764

		2.322724	-12.6268	-0.09207	-10.5436	-0.58947	-11.0764
		2.384658	-12.6724	0.000881	-10.5892	-0.55845	-11.0764
		2.384658	-12.6724	0.093894	-10.6044	-0.49642	-11.0763
		2.415511	-12.7485	0.24878	-10.6956	-0.37236	-11.0763
		2.477283	-12.8702	0.372713	-10.7564	-0.31036	-11.0915
		2.477315	-12.8549	0.434649	-10.802	-0.24832	-11.0914
		2.569713	-13.1592	0.527599	-10.8476	-0.09334	-11.137
		2.569778	-13.1288	0.55855	-10.878	-0.00039	-11.1826
		2.570136	-12.9614	0.6515	-10.9236	0.030592	-11.1978
		2.599427	-13.7678	0.682419	-10.9692	0.154625	-11.2129
		2.599492	-13.7374	0.775305	-11.0452	0.216559	-11.2585
		2.59998	-13.5091	0.806255	-11.0757	0.278559	-11.2737
		2.59998	-13.5091	0.86819	-11.1213	0.371509	-11.3193
		2.600208	-13.4026	0.929994	-11.2277	0.402526	-11.3193
		2.600501	-13.2657	0.991929	-11.2734	0.433477	-11.3497
		2.600924	-13.0679	1.084748	-11.3798	0.588426	-11.4105
		2.601022	-13.0222	1.2397	-11.4406	0.619345	-11.4561
		2.601022	-13.0222	1.332519	-11.547	0.650329	-11.4713
		2.660613	-14.1633	1.394389	-11.6231	0.743312	-11.5017
		2.661329	-13.8286	1.456226	-11.7143	0.805247	-11.5473
		2.661752	-13.6308	1.518161	-11.76	0.836197	-11.5777
		2.691206	-14.3611	1.580095	-11.8056	0.867149	-11.6081
		2.691272	-14.3307	1.641965	-11.8816	0.898034	-11.669
		2.691336	-14.3003	1.827768	-12.0185	0.991017	-11.6994
		2.691466	-14.2394	1.858686	-12.0641	1.021904	-11.7602
		2.691857	-14.0568	2.044524	-12.1857	1.02197	-11.7298
		2.69215	-13.9199	2.137408	-12.2617	1.052855	-11.7906
		2.722515	-14.2242	2.199278	-12.3378	1.083804	-11.821
				2.292065	-12.4594	1.114724	-11.8667
				2.353935	-12.5355	1.176722	-11.8819
				2.415804	-12.6115	1.238691	-11.9123
				2.446365	-12.8245	1.269707	-11.9122
				2.446593	-12.718	1.300626	-11.9579
				2.508267	-12.8854	1.300689	-11.9274
				2.538664	-13.1744	1.362528	-12.0187
				2.53873	-13.144	1.393445	-12.0643
				2.538892	-13.0679	1.455445	-12.0795
				2.569094	-13.4483	1.486331	-12.1404
				2.569257	-13.3722	1.517282	-12.1708
				2.569322	-13.3418	1.548265	-12.186
				2.569551	-13.2353	1.641183	-12.2468
				2.599264	-13.8439	1.672102	-12.2924
				2.599525	-13.7221	1.703053	-12.3228
				2.599752	-13.6156	1.765052	-12.338
				2.599947	-13.5243	1.796004	-12.3684
				2.661068	-13.9503	1.857938	-12.414

				2.691857	-14.0568	1.888889	-12.4444
				2.691955	-14.0112	1.950791	-12.5053
						2.012694	-12.5661
						2.074692	-12.5813
						2.13653	-12.6725
						2.16748	-12.703
						2.198399	-12.7486
						2.260334	-12.7942
						2.260334	-12.7942
						2.353187	-12.8854
						2.35322	-12.8702
						2.38404	-12.9615
						2.384136	-12.9159
						2.445942	-13.0223
						2.476665	-13.1592
						2.47673	-13.1288
						2.476795	-13.0984
						2.476926	-13.0375
						2.507486	-13.2505
						2.507519	-13.2353
						2.507583	-13.2049
						2.538242	-13.3722
						2.538339	-13.3266
						2.567923	-13.996
						2.568053	-13.9352
						2.568151	-13.8895
						2.568216	-13.8591
						2.56828	-13.8287
						2.568379	-13.783
						2.568443	-13.7526
						2.568509	-13.7222
						2.568574	-13.6917
						2.568639	-13.6613
						2.568737	-13.6157
						2.568932	-13.5244
						2.569062	-13.4635
						2.569127	-13.4331
						2.598418	-14.2395
						2.598483	-14.209
						2.598582	-14.1634
						2.598646	-14.1329
						2.598712	-14.1025
						2.598809	-14.0569
						2.629305	-14.3003
						2.629305	-14.3003

References

Alfvén, H. (1942) Existence of electromagnetic-hydrodynamic waves. *Nature*. 150. p. 405.

Aharonian, F., Akhperjanian, A. G., Aye, K.-M., et al. (2005) *A&A*. 435 (17).

Aharonian, F., Akhperjanian, A. G., Bazer-Bachi, A. R., et al. (2006a) *ApJ*. 636. p. 777.

Aharonian, F., Akhperjanian, A. G., Bazer-Bachi, A. R., et al. (2006b) *A&A*. 456. p. 245.

Aharonian, F., Akhperjanian, A. G., Bazer-Bachi, A. R., et al. (2006c) *A&A*. 460. p. 365.

Baade, W. & Zwicky, F. (1934) On super-novae. *Proc. Nat. Acad. Sci.* 20. p. 254-259.

Cocke, W. S., Disney, M. J., & Taylor, D. J. (1969) *Nature.* 221. p. 525-527.

Gaensler, B. M. & Slane, P. O. (2006) *ARA&A*. 44. p. 17.

Hester, J. Jeff (2008) The Crab Nebula: An Astrophysical Chimera. *ARAA.* **46** (1). p. 127–155.

Hewish, A., Bell, S. J., Pilkington, J. D. H., Scott, P. F. & Collins, R. A. (1968) Observation of a rapidly pulsating radio source. *Nature*. 217. p. 709-713.

Hobbs, M. (2014) *An Introduction to Pulsars*. [Online] Available from: http://www.atnf.csiro.au/outreach/education/everyone/pulsars/index.html [Accessed: 24th March 2014]

Imagine (2014) IMAGINE THE UNIVERSE!. [Online] Available from: http://imagine.gsfc.nasa.gov/science/objects/pulsars2.html[Accessed: 25th March 2014]

Lyne, A. G. & Smith, F. G. (1990) *Pulsar Astronomy*. Cambridge University Press.

Manchester, R. N. & Taylor, J. H. (1977) Pulsars., ed. Smith F. G.

Mattana, F., Falanga, M., Gotz, D., et al. (2009) THE EVOLUTION OF THE γ - AND X-RAY LUMINOSITIES OF PULSAR WIND NEBULAE. *ApJ.* 694. P. 12-17.

Mayer, M., Brucker, J., Holler, M., Jung, I., Valerius, K. & Stegmann, C. (2013) Predictimg the X-ray flux of evolved pulsar wind nebulae based on VHE γ ray observations. arXiv:1202.1455v3

Minkowski, R. (1942) *ApJ.* 96. p.199-213.

Oppenheimer, J. R. & Volkoff, G. (1939) On massive neutron cores. *Phys. Rev.* 55. p. 374-381.

Pacini, F. (1967) Energy emission from a neutron star. *Nature*. 216. p. 567-568.

Pacini, F. & Salvati, M. (1973) ApJ. 186. p. 249.

Richards, D. W. & Comella, J. M. (1969) *Nature*. 222. p. 551-552.

Staelin, D. H. & Refenstein, E. C. (1968) *Science* 162. p. 1481-1483.

TeVCat (2014) *Welcome to TeVCat!*. [Online] Available from: http://tevcat.uchicago.edu/ [Accessed: 29th March 2014]

Zeilik, M. and Gaustad, J. (1990) Astronomy: The Cosmic Perspective. *New York: John Wiley & Sons, Inc*. p. 544.

List of Publications

1. A method to estimate the cooling time of ultra-relativistic electrons in Pulsar Wind Nebulae, K L I Gunawardhana, A U Abeysekara, K P S C Jayaratne, and J Adassuriya, 70th Proc. Sri Lanka Assoc. Advmt. Sci., E1-827,Dec. 2014.